

Review

# Molybdenum Disulfide as Tunable Electrochemical and Optical Biosensing Platforms for Cancer Biomarker Detection: A Review

Ziyue Qin <sup>1,2</sup>, Jiawei Zhang <sup>1,2</sup> and Shuang Li <sup>1,2,\*</sup> 

<sup>1</sup> Medical College, Tianjin University, Tianjin 300072, China; 2021235042@tju.edu.cn (Z.Q.); jiawei\_zhang@tju.edu.cn (J.Z.)

<sup>2</sup> Academy of Medical Engineering and Translational Medicine, Tianjin University, Tianjin 300072, China

\* Correspondence: lishuangv@tju.edu.cn; Tel./Fax: +86-022-83612122

**Abstract:** Cancer is a common illness with a high mortality. Compared with traditional technologies, biomarker detection, with its low cost and simple operation, has a higher sensitivity and faster speed in the early screening and prognosis of cancer. Therefore, extensive research has focused on the development of biosensors and the construction of sensing interfaces. Molybdenum disulfide (MoS<sub>2</sub>) is a promising two-dimensional (2D) nanomaterial, whose unique adjustable bandgap shows excellent electronic and optical properties in the construction of biosensor interfaces. It not only has the advantages of a high catalytic activity and low manufacturing costs, but it can also further expand the application of hybrid structures through different functionalization, and it is widely used in various biosensors fields. Herein, we provide a detailed introduction to the structure and synthesis methods of MoS<sub>2</sub>, and explore the unique properties and advantages/disadvantages exhibited by different structures. Specifically, we focus on the excellent properties and application performance of MoS<sub>2</sub> and its composite structures, and discuss the widespread application of MoS<sub>2</sub> in cancer biomarkers detection from both electrochemical and optical dimensions. Additionally, with the cross development of emerging technologies, we have also expanded the application of other emerging sensors based on MoS<sub>2</sub> for early cancer diagnosis. Finally, we summarized the challenges and prospects of MoS<sub>2</sub> in the synthesis, functionalization of composite groups, and applications, and provided some insights into the potential applications of these emerging nanomaterials in a wider range of fields.



**Citation:** Qin, Z.; Zhang, J.; Li, S. Molybdenum Disulfide as Tunable Electrochemical and Optical Biosensing Platforms for Cancer Biomarker Detection: A Review. *Biosensors* **2023**, *13*, 848. <https://doi.org/10.3390/bios13090848>

Received: 26 July 2023

Revised: 22 August 2023

Accepted: 23 August 2023

Published: 25 August 2023



**Copyright:** © 2023 by the authors. Licensee MDPI, Basel, Switzerland. This article is an open access article distributed under the terms and conditions of the Creative Commons Attribution (CC BY) license (<https://creativecommons.org/licenses/by/4.0/>).

**Keywords:** molybdenum disulfide; electrochemical sensor; optical sensor; cancer biomarkers; detection

## 1. Introduction

Cancer is the world's leading cause of death and the second most common disease [1]. At present, more than 200 types of cancers have been found. In general, imaging technologies such as ultrasound, positron emission tomography (PET), magnetic resonance imaging (MRI), and computed tomography (CT) are used for early screening, followed by confirmation through tissue biopsy and histology, so that patients can be treated in a timely manner, which can dramatically reduce cancer mortality [2–4]. However, traditional cancer detection methods are often invasive, expensive, complex, and time consuming. Rapid diagnosis and early prevention are crucial for the clinical treatment and management of cancer [5]. Cancer biomarkers, as important components of detection, prognosis, and providing an etiological analysis of cancer, are abnormal quantities of biological molecules generated by the body's response to the disease or directly by the cancer tumor itself, including DNA, RNA, genes, proteins, enzymes, peptides, exosomes, and metabolomics [6]. So far, the main cancer biomarkers that have been discovered include carcinoembryonic antigen (CEA), carbohydrate antigen 125 (CA125), carbohydrate antigen 15-3 (CA15-3), human epidermal growth factor receptor 2 (HER2), vascular endothelial growth factor 165

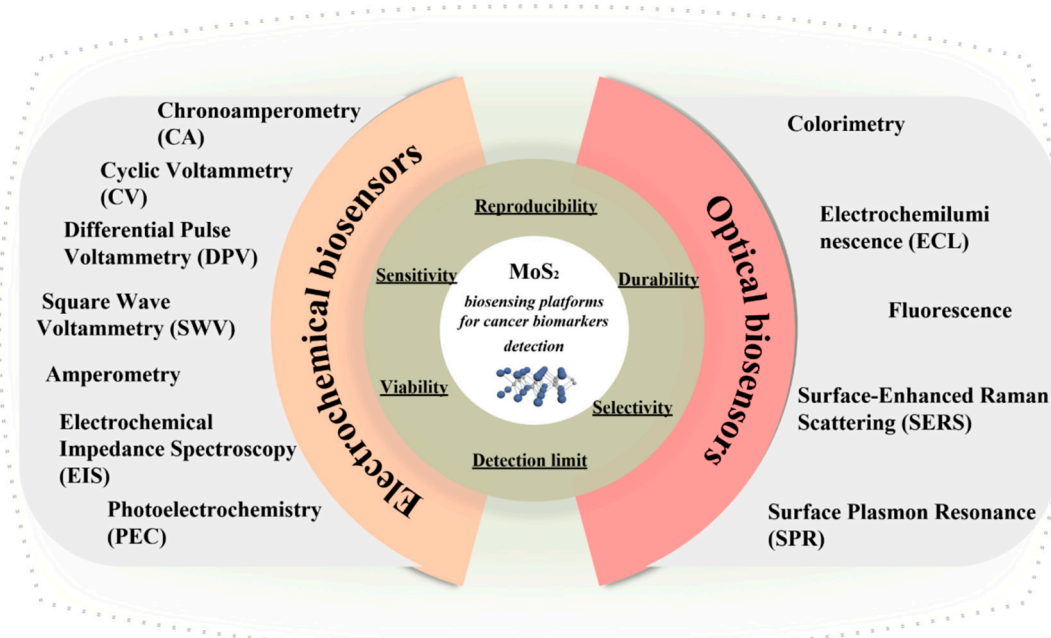
(VEGF<sub>165</sub>), tissue-specific antigen (TPS), prostate-specific antigen (PSA), alpha-fetoprotein (AFP), squamous cell carcinoma antigen (SCCA), circulating tumour cells (CTCs), microRNAs, and exosomes [7]. They typically exist in the blood, urine, tears, oral fluids, and other tissues [8]. Cancer biomarker detection has accelerated the process of cancer diagnosis, and can obtain higher sensitivity and faster cancer screening. Enzyme-linked immunosorbent assay (ELISA) [9], polymerase chain reaction (PCR) [10], clustered regularly interspaced short palindromic repeats Cas9 (CRISPR-Cas9) [11], loop-mediated isothermal amplification (LAMP), time-resolved fluorescence spectroscopy (TR-FS), radioimmunoassay (RIA), and electrophoresis [12] have been used for the detection of cancer biomarkers [13]. In addition, emerging technologies such as artificial intelligence, long read sequencing, microarrays, DNA methylation, and liquid biopsy are also committed to the development and high throughput profiling of many biomarkers to strengthen cancer management and improve early screening [14,15].

In recent years, compared with traditional technologies, biosensors have potential advantages such as a high sensitivity and selectivity, high accuracy, low cost, fast detection, high stability, availability, and ease of operation. They play an important role in diagnosing and quantitatively analysing biomarker concentrations, and are widely used in various fields such as healthcare, food inspection, and environmental testing [16]. Biosensors use various biomolecules as biometric recognition components, which are fixed on the sensor surface and converted into measurable electronic or optical signals through biological responses with the detection target substance for cancer biomarker detection [17]. Biosensors can be divided into electrochemical, optical, mass-dependent, and radiation sensitive biosensing platforms based on different transduction principles [18,19]. Developing efficient and practical biosensors usually requires consideration of the following aspects: (1) synthesis, manufacture, and assembly of suitable sensing materials; (2) selecting appropriate recognition or capture molecules; and the (3) integration of sensor surfaces with biomolecules [20,21]. With the development of nanotechnology in medicine and biotechnology, more and more researchers are combining different types of nanomaterials with optical, electrical, mechanical, and magnetic sensors to design nanosensors for the detection of cancer biomarkers [22]. Nanobiosensors are generally composed of nanomaterials and a sensor based on biometric recognition elements [23]. They can be combined according to the interaction of the affinity bond, covalent bond, cross-linking, capture, and physical adsorption [24].

Among the various nanomaterials, 2D-layered nanomaterials have attracted widespread research interest due to their quantum confinement, high absorption coefficient, high specific surface area, and tunable bandgap characteristics [25]. Among them, graphene has excellent physical properties, chemical adjustability, and application potential, and its synthesis, properties, and applications are widely known [26]. The impressive performance of graphene in various fields has aroused strong interest in the exploration of a wider range of 2D-layered nanomaterials “beyond graphene” [27]. Transition metal dichalcogenides (TMDs), as a new class of stable inorganic graphene analogues, have been further studied. Among them, MoS<sub>2</sub> is regarded as a representative of TMDs. Its single molecular layer is composed of an atomic layer of transition metal Mo sandwiched between two sulfur elements S [28]. Mo atoms and S atoms are closely connected by forming a strong covalent bond through coordination, and the interlayer is connected by a weak van der Waals force. This weak connection mode between layers provides conditions for MoS<sub>2</sub> stripping to form a single-layer 2D planar structure [29], showing unique electronic, optical, mechanical, and chemical properties [30–32]. Most importantly, due to the confinement of electrons/holes in ultra-thin planar structures, MoS<sub>2</sub> is highly sensitive to changes in the microenvironment [33], thus exhibiting advantages in the construction of biosensing interfaces [34,35].

A large number of literature works have reported that different types of biosensing platforms based on MoS<sub>2</sub> are used to detect various biomarkers, considering the needs of cancer biomarker detection in terms of high sensitivity, high reproducibility, easy pro-

cessing, low cost, and miniaturization. In this work, we comprehensively reviewed and summarized the application of electrochemical/optical sensing platforms based on MoS<sub>2</sub> in cancer biomarker detection, and highlighted the excellent characteristics and application performance of MoS<sub>2</sub> and its composite structures (Scheme 1). Firstly, the research status of early cancer diagnosis and traditional/emerging biosensing technologies for cancer biomarkers detection were investigated, with a focus on introducing 2D nanomaterials represented by MoS<sub>2</sub>. Secondly, the structures and synthesis methods of MoS<sub>2</sub> were discussed in detail, as well as the unique properties and advantages/disadvantages exhibited by different structures. Then, the focus was on summarizing the recent electrochemical and optical sensing work of MoS<sub>2</sub> and its composite structures in the field of cancer biomarker detection. In addition, we expanded the application of other emerging sensors based on MoS<sub>2</sub> for early cancer diagnosis. Finally, we summarized the challenges and prospects of MoS<sub>2</sub> in terms of the synthesis, functionalization of composite groups, and applications, and provided some insights into the enormous potential of these emerging 2D nanomaterials in the field of cancer biomarkers detection.



**Scheme 1.** Electrochemical/optical sensing platforms based on MoS<sub>2</sub> in cancer biomarker detection.

## 2. Synthesis and Characteristics of Molybdenum Disulfide

MoS<sub>2</sub> has a hexagonal lattice structure, with three common crystal structures of 1T, 2H, and 3R, and their corresponding point groups are D6d, D6h, and C3v [36]. In addition, an additional hypothetical 2T structure of MoS<sub>2</sub> has been studied and reported [37]. Accordingly, 1, 2, and 3 represent the number of layers, T represents the trigonal configuration, H represents the hexagonal configuration, and R represents the rhombohedral configuration. As shown in Figure 1a, the MoS<sub>2</sub> layers in the 2H, 3R, 1T, and additional 2T crystal structures are arranged in anti-parallel AB, parallel ABC, parallel AA, and anti-parallel AA' stacking sequences, respectively [38]. The properties of MoS<sub>2</sub> may show different characteristics according to the change in crystal structure [39]. Among these crystal structures, 2H-MoS<sub>2</sub> exhibits thermal stability and semiconductor characteristics, making it the most widely used in practical applications. While 1T-MoS<sub>2</sub> shows paramagnetism and metallicity [40], it shows metastability and is easy to convert into 2H-MoS<sub>2</sub>, which facilitates the photoelectric application of MoS<sub>2</sub> [41]. In addition, the number of layers can also alter the electrical and optical properties of MoS<sub>2</sub> nanosheets. For example, reducing the thickness of MoS<sub>2</sub> nanosheets can improve conductivity and accelerate the electron transfer

rate [42]. The application of MoS<sub>2</sub> in electronic devices is inseparable from its electronic band structure and electronic properties that are dependent on the density of states. Kuc et al. calculated the electronic band structure of MoS<sub>2</sub>, and obtained the electronic band structure diagram of MoS<sub>2</sub> with different thicknesses (Figure 1b). The indirect band gap of blocky MoS<sub>2</sub> is 1.2 eV. During the change from a blocky structure to a layered structure, the band gap thickness gradually increases (1.2–1.9 eV) and transforms from indirect to direct band gap (1.9 eV), showing good absorption and photoluminescence characteristics [43,44]. Compared with graphene with a 0 eV band gap, this adjustable band gap improves the application of MoS<sub>2</sub> materials in the field of optoelectronics [45]. The key reason for the widespread application of MoS<sub>2</sub> in optoelectronics is that it exhibits tunable band gap characteristics as it changes in size and structure. Different band gaps bring adjustable optical responsiveness, specific detection rate, and response time, thus having a wide range of applications [46].

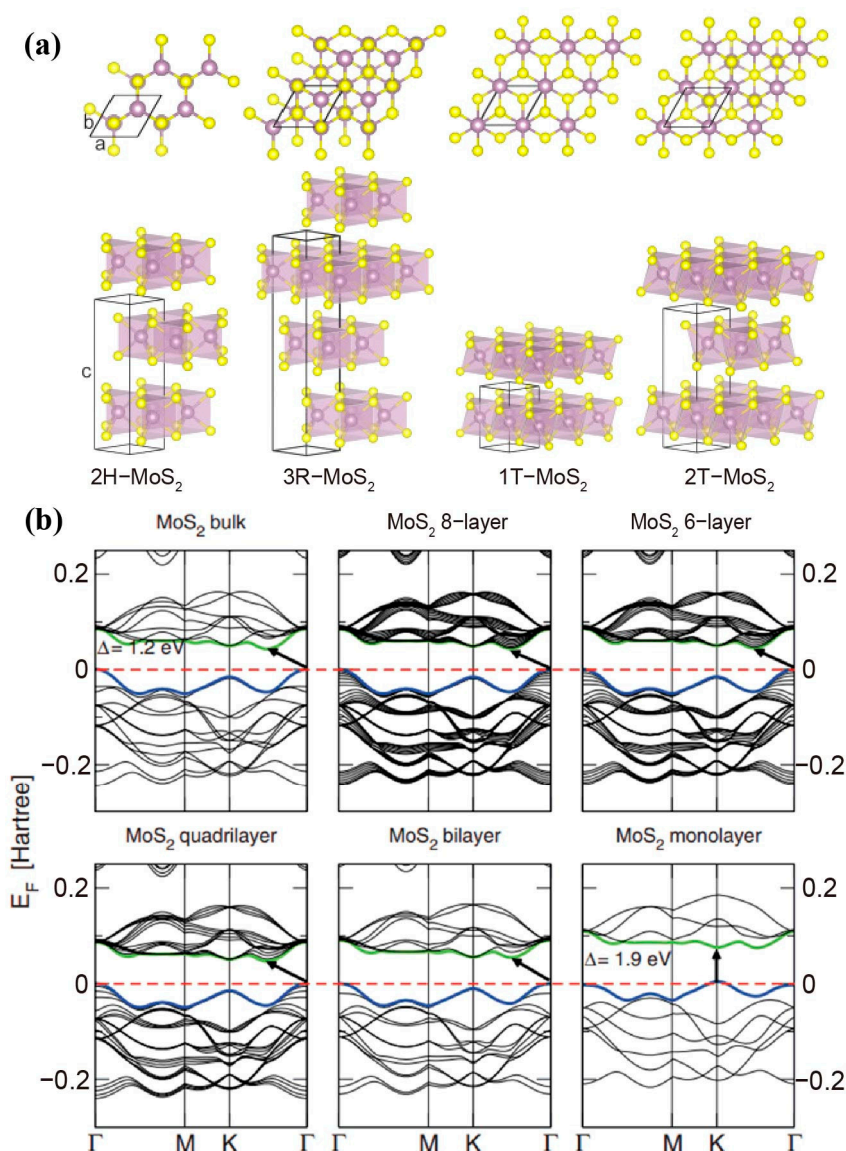


**Figure 1.** (a) Various crystal structures of MoS<sub>2</sub> (1T, 2H, 3R, and 2T) [38]. Copyright 2014, Elsevier. (b) Electronic band structure diagram of MoS<sub>2</sub> with different thicknesses [44]. Copyright 2011, American Physical Society.

By controlling the synthesis conditions of MoS<sub>2</sub>, various nanostructures can be synthesized. In addition to the most widely used 2D MoS<sub>2</sub> nanosheets [47], these also include

structures such as 0D quantum dots (QD) [48], 1D (nanotubes) [49], and 3D (nanoflowers) [50]. Various structures exhibit different characteristics, such as the direct band gap of nanosheets, photoluminescence of quantum dots, and the high surface area and volume ratio of nanoflowers, which make MoS<sub>2</sub> exhibit a unique and excellent performance in different application scenarios [51]. The synthesis methods of MoS<sub>2</sub> can be roughly divided into two categories: top-down and bottom-up (Figure 2). The top-down methods mainly include mechanical exfoliation, liquid-phase exfoliation, and chemical methods. The bottom-up methods mainly include chemical vapor deposition (CVD) and solvothermal or hydrothermal methods [52].

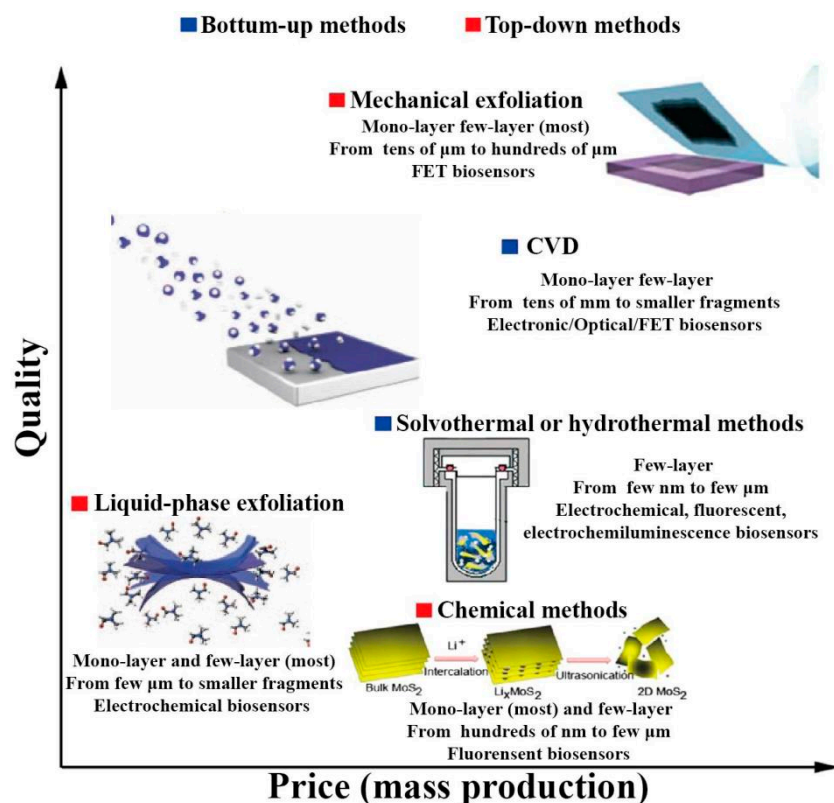


**Figure 2.** Synthesis methods of MoS<sub>2</sub> [27,53]. Copyright 2017, Elsevier. Copyright 2012, Springer Nature.

### 2.1. Top-Down Methods

**Mechanical exfoliation:** As the MoS<sub>2</sub> layers are connected by a weak van der Waals force, the layered MoS<sub>2</sub> can be easily peeled off by friction of the bulk substrate MoS<sub>2</sub> with tape. The peeled tape is pressed into the appropriate substrate, and the synthetic process of MoS<sub>2</sub> mechanical exfoliation is completed by using the van der Waals force formed between MoS<sub>2</sub> and the substrate. The mechanical exfoliation is limited by its low yield and thus cannot be used for large-scale production. However, this method can produce layered MoS<sub>2</sub> with an ideal purity and large transverse size, and is often used as a laboratory preparation method for studying the properties of MoS<sub>2</sub> materials [54].

**Liquid-phase exfoliation:** In order to overcome the low yield and difficulty in the large-scale production of mechanical exfoliation, the process of stripping MoS<sub>2</sub> in solution is called liquid-phase exfoliation. Specifically, the bulk MoS<sub>2</sub> is dissolved in a suitable solution and separated from the layered MoS<sub>2</sub> by methods such as bubbling, ultrasonic dispersion, grinding, and shearing [55–58]. Among them, adding surfactants [59] or bubbling bubbles [60] in the solution can help improve the stability of MoS<sub>2</sub>, effectively maintain the layered structure of MoS<sub>2</sub> after peeling, and prevent it from recombining with

the bulk MoS<sub>2</sub>. Overall, liquid-phase exfoliation is simpler and more cost-effective than mechanical exfoliation, making it stand out in industrial applications [61].

**Chemical methods:** Chemical methods mainly rely on metal ions entering the inter-layer of bulk MoS<sub>2</sub> to achieve the detachment of MoS<sub>2</sub> [62]. In the chemical stripping process, the most widely used metal ion reported is Li<sup>+</sup>. However, the intercalation of Li<sup>+</sup> will simultaneously lead to the transfer of MoS<sub>2</sub> from the 2H phase exhibiting semiconductor properties, to the 1T phase exhibiting metal properties, which limits the application scenarios of the generated MoS<sub>2</sub>. Further research has shown that annealing at 300 °C can restore MoS<sub>2</sub> formed by Li<sup>+</sup> intercalation to the 2T phase [63]. Electrochemical methods have also emerged in the MoS<sub>2</sub> stripping process, typically using block MoS<sub>2</sub> as the cathode to achieve stripping. However, the large size and area of MoS<sub>2</sub> produced by electrochemical stripping methods are limited in their application in the biological field, thus requiring more exploration [64].

## 2.2. Bottom-Up Methods

**CVD:** CVD is a typical nanomaterial growth technique that can be used to prepare high-quality MoS<sub>2</sub> with scalable size, controllable thickness, and excellent electronic properties [65]. CVD uses precursor gas molecules to adsorb on the substrate surface and generate a thermal chemical decomposition reaction, thus forming high-quality layered MoS<sub>2</sub>. At present, Mo precursors commonly used in CVD mainly include Mo and Molybdenum trioxide, while S precursors mainly use hydrogen sulfide gas or vaporized S [66,67]. On this basis, we further studied the CVD process of MoS<sub>2</sub> using Molybdenum (V) chloride as a precursor. The characterization results verified that this precursor can produce a larger area of high-quality single-layer MoS<sub>2</sub> films, but more precursors that can be used for CVD still need to be further explored [68]. CVD can not only produce MoS<sub>2</sub> with a high film quality, but also easily functionalize MoS<sub>2</sub> by introducing other precursors during the preparation process. The entire process is very simple and convenient, and is commonly used for studying the properties of MoS<sub>2</sub> materials and constructing biosensors [69].

**Solvothermal or hydrothermal methods:** Solvothermal or hydrothermal methods are a simple, scalable, and easily controllable method for preparing MoS<sub>2</sub>. The solvothermal method commonly uses solid precursors, while the hydrothermal method commonly uses liquid precursors [70]. Generally, under high temperature conditions, the molybdate that provides the Mo source and the sulfides that provide the S source are reacted in a polytetrafluoroethylene high-pressure reactor, and MoS<sub>2</sub> is synthesized through the generated steam pressure. In most cases, an annealing treatment is required to improve its crystal quality and purity [71]. This method can effectively preserve the 2H phase of MoS<sub>2</sub> and achieve control of the size parameters of MoS<sub>2</sub> to a certain degree. The harmless preparation process further preserves the biocompatibility of MoS<sub>2</sub>, making it easier to obtain smaller microcrystals with high catalytic activity compared to CVD. It has great potential in constructing electrochemical and fluorescent biosensors [72].

In addition to the above methods, there are also some methods for the preparation of MoS<sub>2</sub>, such as physical vapor deposition (PVD), sputtering, vapor solid growth, etc. Due to the different principles and processes of preparation methods, the generated MoS<sub>2</sub> exhibits different characteristics and is applied in different scenarios accordingly. The large size of MoS<sub>2</sub> prepared by mechanical exfoliation limits its biosensing applications. Similarly, PVD exhibits harmful reverse defects compared with CVD during functionalization, which also affects its application range. Correspondingly, CVD and solution chemistry processes have been more widely promoted due to their adjustable preparation process and high-quality synthesis of MoS<sub>2</sub>. The construction of electrochemical/optical sensors using the electrical/optical properties of MoS<sub>2</sub> has been extensively reported.

## 3. Electrochemical Biosensors for Cancer Biomarkers Detection Based on MoS<sub>2</sub>

Electrochemical sensors are mainly composed of sensitive components, signal transduction components, and nano modified electrode structures. Electrochemical analysis

technology is an important detection method in the field of biomedicine. Its basic principle is to analyse the changes in current or impedance signals generated by the interaction between the analyte and the electrode surface. It can monitor the charge movement between reaction interfaces and has significant advantages through its fast response [73]. In recent years, sensitive electrochemical biosensors have been developed for the detection of cancer biomarkers [74]. MoS<sub>2</sub> has a hexagonal lattice layered structure, which gives it excellent properties such as a high specific surface area, high electron mobility, thermal stability, catalytic activity, and diamagnetism, which is commonly used in semiconductor materials, catalysts, and lubricating materials, etc. [75–77]. The unique adjustable bandgap characteristic of MoS<sub>2</sub> provides excellent photoluminescence properties, which are widely used in optical devices such as photodetectors. Additionally, MoS<sub>2</sub>, as a promising emerging nanomaterial, has low manufacturing costs, rich nanostructures, and is easy to functionalize, making it form hybrid structures with other precious metal nanomaterials, which is widely used in the field of electrochemical sensing [78]. In this chapter, we divide electrochemical biosensors into potentiometry, amperometry, impedimetry, and photoelectrochemical (PEC) biosensors according to different signal transductions, and introduce the latest application progress of MoS<sub>2</sub> in cancer biomarker detection.

### 3.1. Potentiometry

Potentiometric sensors obtain information about analytes by measuring the current when potential changes, mainly including chronoamperometry (CA), cyclic voltammetry (CV), differential pulse voltammetry (DPV), and square wave voltammetry (SWV), which are widely used electrochemical analysis methods. These methods fix the biometric elements (such as antibodies, enzymes and aptamers) on the electrode surface, and monitor the current changes triggered when the analyte combines with the biometric element when the potential between the working electrode and the reference electrode remains constant. Within the linear potential range, the monitored peak current value is directly related to the concentration of the target analyte in the solution, so as to realize the detection of the target.

The electronic properties of MoS<sub>2</sub> are highly dependent on its phase structure. The ultra-thin MoS<sub>2</sub> has a good performance, but it is difficult to maintain stability in an independent state and is easy to aggregate [79]. In order to improve this problem, Ying et al. [80] used liquid-phase exfoliation and surface modification to synthesize 2H-MoS<sub>2</sub> (Figure 3a), and used platinum nanowire (Pt NWs) arrays as nanopillars, which were added to the ultra-thin 2D MoS<sub>2</sub> interlayer to form Pt NWs arrays@MoS<sub>2</sub> nano hybrid, which improved the specific surface area and porosity, and could be used as “electronic wires” to catalyze electron transfer at the interface, avoiding folding by creating new dimensions. Thus, stability and current signal enhancement were achieved.

Two main reasons that limit the practical application of MoS<sub>2</sub> in electrochemical sensing are that the strong van der Waals force effect between layers, which leads to aggregation and relatively low conductivity in layers [81]. In order to overcome these shortcomings, Su et al. [82] synthesized ionic liquid (IL) functionalized AuNPs/MoS<sub>2</sub>/rGO nanocomposites for sensitive detection of cancer-specific target nucleolin (Figure 3b). The linear range of the unlabeled electrochemical sensor obtained was 0.5 nM–1.0 μM, and the detection limit was 0.16 nM. Graphene has a large π electronic structure and edge, because of the synergistic effect, and the combination of MoS<sub>2</sub> and graphene can significantly improve the conductivity and large surface area of MoS<sub>2</sub> [83]. In addition, the introduction of AuNPs into nanocomposites can not only fix the thioaptamer through the Au-S bond, which improves the affinity and specificity, but it can also enhance electron transfer and amplify the electrochemical signal.

Song et al. [84] modified rGO/MoS<sub>2</sub>@polyaniline nanosheets of 3D arrays on the surface of the Au electrode and further incubated carcinoembryonic antigen (CEA)-specific antibodies to achieve high sensitivity detection of CEA (Figure 3c). First, the sensor combines rGO with MoS<sub>2</sub> to improve the stack phenomenon of MoS<sub>2</sub>, thus effectively enhancing the electron transfer efficiency of the electrode. Then, polyaniline was further embedded

to introduce a large number of amino groups that can bind to CEA specific antibodies, and CEA was detected using CV in a wide linear range (0.001–80 ng/mL), with a limit of detection (LOD) of 0.3 pg/mL. Gui et al. [85] synthesized ce-MoS<sub>2</sub>/AgNR composites by using the van der Waals force and electrostatic interaction between chemically exfoliate MoS<sub>2</sub> nanosheets (ce-MoS<sub>2</sub>) and Ag nanorods (AgNRs). Because of the synergistic effect, the conductivity of ce-MoS<sub>2</sub>/AgNR composites increased by nearly twice. The prepared unlabeled electrochemical immunosensor (EI) can sensitively detect prostate-specific antigen (PSA) in a wide linear range (0.1–1000 ng/mL) (Figure 3d), with a detection limit as low as 0.051 ng/mL, and could have broad application potential in the clinical diagnosis of prostate cancer.

### 3.2. Amperometry

Amperometric sensors achieve quantitative detection of analytes by applying a constant voltage to the sensing platform to detect the current generated by the conversion of corresponding electroactive substances. Because of their convenience and high accuracy, they are widely used in the detection of cancer biomarkers. As a result of the excellent catalytic activity of MoS<sub>2</sub> for the reduction in H<sub>2</sub>O<sub>2</sub>, Ma et al. [86] used the hydrothermal method to combine MoS<sub>2</sub> nanoflowers (MoS<sub>2</sub> NFs) with p-type metal semiconductor oxide cuprous oxide (MoS<sub>2</sub>@Cu<sub>2</sub>O) (Figure 4a), and, at the same time, the introduction of AuNPs generated MoS<sub>2</sub>@Cu<sub>2</sub>O-Au complexes by Au-S bonds as nanoprobe for signal amplification. The constructed sandwich immunosensor could detect the cancer marker alpha fetoprotein (AFP) of primary liver cancer in the wide linear range of 0.1 pg/mL to 50 ng/mL, demonstrating good application prospects. Ma et al. [87] prepared a sandwich-type electrochemical immunosensor for the sensitive detection of CEA by coupling tri-metallic yolk-shell Au@AgPt nanocubes (Au@AgPt YNCs) loaded on amino-functionalized MoS<sub>2</sub> NFs (MoS<sub>2</sub> NFs/Au@AgPt YNCs) with secondary antibodies (Figure 4b). As a result of the biphasic synergistic catalysis, the synthesized MoS<sub>2</sub> NFs/Au@AgPt YNCs as a signal label effectively catalyzed the reduction of H<sub>2</sub>O<sub>2</sub> to amplify the current signal, and realized the high-precision detection of CEA in the range of 10 fg/mL–100 ng/mL, with an LOD as low as 3.09 fg/mL (S/N = 3). These works provide ideas for the composite modification of MoS<sub>2</sub> with different nano forms and further applications in biosensing platforms.

### 3.3. Impedimetry

Impedance sensors are an important type of electrochemical sensing that obtains information about analytes by measuring the conductance through interface reactions on the electrode surface. This type of sensor is very sensitive to the change in electrode, and is in an advantageous position in the detection of biomarkers. Therefore, it is also widely introduced into the construction of the electrochemical sensing platform for the detection of cancer biomarkers. Jia et al. [88] prepared a novel nanohybrid of polyoxometalate-derived MoS<sub>2</sub> nanosheets (pd-MoS<sub>2</sub> NSs) using a hydrothermal method, which exhibited an excellent electrochemical activity and abundant catalytic sites. Furthermore, pd-MoS<sub>2</sub> NSs were vertically grown over β-FeOOH NRs (pd-MoS<sub>2</sub>@β-FeOOH), serving as complementary DNA platforms for fixing oncogenes and tumour suppressor miRNA-21, using electrochemical impedance spectroscopy (EIS) to detect miRNA-21, with an LOD as low as 0.11 fM. In addition, microfluidic electrochemical immunochips have been evaluated as a powerful detection platform because of their high sensitivity, low cost, portability, and easy miniaturization. Sri et al. [89] synthesized MoS<sub>2</sub> NFs using the same method, and electrophoretically deposited them on an indium tin oxide (ITO)-coated glass substrate. Because of the morphology of MoS<sub>2</sub> NFs, antibodies can be effectively fixed on the electrode surface through physical adsorption. The biosensor can sensitively detect tumour necrosis factor-α (TNF-α) between 1–200 pg/mL, with an LOD as low as 0.202 pg/mL (Figure 4c). Hu et al. [90] first prepared MoS<sub>2</sub> by liquid-phase exfoliation and formed a hybrid film with PDDA, designed a three-electrode system in the microfluidic chip, and introduced a MoS<sub>2</sub>/PDDA film modified with anti-AFP as the working electrode, Ag/AgCl as the

reference electrode, and ITO as the counter electrode (Figure 4d). The linear range of AFP detected by EIS was 0.1 ng/mL to 10 ng/mL, with an LOD of 0.033 ng/mL.

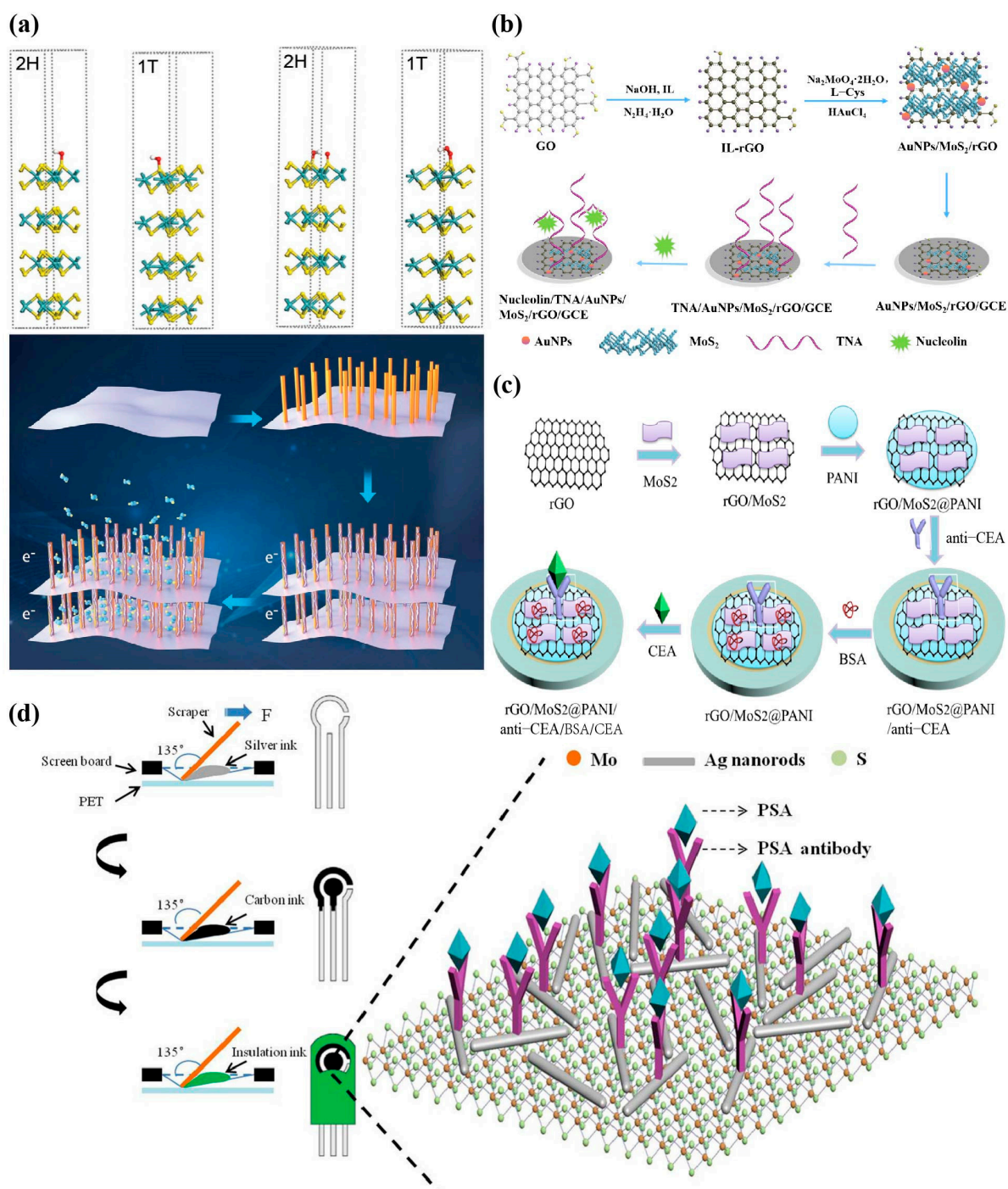


**Figure 3.** Examples of potentiometric sensors used for detecting various cancer biomarkers. (a) Optimized structure of 2H–MoS<sub>2</sub> and 1T–MoS<sub>2</sub> (upper plate) and schematic diagram using Pt NWs arrays as nanopillars in ultra-thin MoS<sub>2</sub> films (lower plate) [80]. Copyright 2020, Wiley. (b) Schematic illustration for the synthesis of the AuNPs/MoS<sub>2</sub>/rGO nanocomposite and nucleolin electrochemical aptasensor strategy [82]. Copyright 2020, Elsevier. (c) Schematic diagram of highly sensitive detection of CEA based on rGO/MoS<sub>2</sub>@polyaniline nanosheets of 3D arrays [84]. Copyright 2020, Elsevier. (d) Schematic illustration of the fabrication and PSA detection process of EI [85]. Copyright 2020, Springer Nature.

### 3.4. Photoelectrochemistry (PEC)

PEC utilizes photosensitive materials at the electrode interface as signal converters to analyse the electrical signals generated by analytes under light irradiation, combining the advantages of spectral analysis and electrochemical technology. MoS<sub>2</sub> exhibits excellent characteristics of a tunable bandgap in its transition from a blocky structure to a layered structure. The quantum confinement effect led to good visible light absorption and photoelectric conversion efficiency of layered MoS<sub>2</sub> as a direct bandgap semiconductor under visible light excitation, resulting in photocurrent generation. Therefore, it has been introduced into the application of photoelectrochemical sensing platforms. Hu et al. [91] utilized this mechanism to design a PEC sensing platform based on MoS<sub>2</sub>/Au/GaN for the high sensitivity detection of AFP (Figure 4e). MoS<sub>2</sub> can suppress the charge transfer of Au/GaN photoelectrodes, leading to a significant decrease in photocurrent. However, the presence of AFP can reduce the inhibitory effect on the photocurrent, thereby utilizing the difference in photocurrent to detect AFP. AFP detection is achieved in a wide linear range of 1.0–150 ng/mL, with an LOD of 0.3 ng/mL. This method has a good sensitivity and high selectivity for AFP detection. Wei et al. [92] synthesized a light-responsive ZnS/C/MoS<sub>2</sub> nanocomposite to construct a PEC immunosensor for detecting CEA, with a linear range of 2.0 pg/mL–10.0 ng/mL and an LOD of 1.30 pg/mL (S/N = 3), showing good analytical characteristics (Figure 4f). In addition to the above sensing methods, other sensing methods based on MoS<sub>2</sub> are listed in Table 1 to detect various cancer biomarkers.

**Table 1.** Electrochemical biosensors for cancer biomarkers detection based on MoS<sub>2</sub>.

Method	Analytes	Electrode/Label	Linear Range	LOD	Ref.
Chronoamperometry	AMACR	Pt NWs array@2H-MoS <sub>2</sub> /SPE	0.70–12.50 ng/μL	0.5 pg/μL	[80]
CV	CEA	Ab/rGO/MoS <sub>2</sub> @PANI/GCE	0.001–80 ng/mL	0.3 pg/mL	[84]
CV	PSA	Ab/ce-MoS <sub>2</sub> /AgNR/SPE	0.1–1000 ng/mL	0.051 ng/mL	[85]
DPV	CEA	Ab/MoS <sub>2</sub> -PBNCs/GCE	0.005–10 ng/mL	0.54 pg/mL	[93]
DPV	CEA	Ag/MoS <sub>2</sub> @Fe <sub>3</sub> O <sub>4</sub> - Ab2/CEA/Ab1/Ag/MGCE	0.0001–20 ng/mL	0.03 pg/mL	[94]
DPV	miRNA-182	ssRNA/MoS <sub>2</sub> /Ti <sub>3</sub> C <sub>2</sub> /GCE	1 fM–0.1 nM	0.43 fM	[95]
DPV	CEA	MoS <sub>2</sub> -AuNPs/HRP- Ab2/CEA/Ab1/MoS <sub>2</sub> - AuNPs/GCE	10 fg/mL–1 ng/mL	1.2 fg/mL	[96]
DPV	Nucleolin	TNA/AuNPs/MoS <sub>2</sub> /rGO/GCE	0.5 nM–1.0 μM	0.16 nM	[82]
DPV	CEA	Ab/Pd@Pt/MoS <sub>2</sub> -Gr/GCE	0.00001–100 ng/mL	0.005 pg/mL	[97]
DPV	CA125	Ab/CuBTC@MoS <sub>2</sub> -AuNPs/SPE	0.5 mU/mL–500 U/mL	0.5 mU/mL	[98]
DPV	anti-retroviral agent indinavir	ZnO NRs/MoS <sub>2</sub> NSs/SPE	0.01–0.66 μM & 0.66–7.88 μM	0.007 μM	[99]
SWV	CEA	CeO <sub>2</sub> -MoS <sub>2</sub> -Pb <sup>2+</sup> - Ab2/CEA/Ab1/AuNPs/GCE	0.001–80 ng/mL	0.3 pg/mL	[100]
Amperometry	CEA	Ab/Ag/MoS <sub>2</sub> /rGO/GCE	0.01 pg/mL–100 ng/mL	1.6 fg/mL	[101]
Amperometry	HBeAg	Au@Pd/MoS <sub>2</sub> @MWCNTs- Ab2/HBeAg/Ab1/p- GO@Au/GCE	0.1–500 pg/mL	26 fg/mL	[102]
Amperometry	AFP	MoS <sub>2</sub> @Cu <sub>2</sub> O-Au- Ab2/AFP/Ab1/AuNPs/GCE	0.1 pg/mL–50 ng/mL	0.037 pg/mL	[86]
Amperometry	AFP	Ab/Pt NDs/PDDA/MoS <sub>2</sub> @PPy NTs/GCE	50 fg/mL–50 ng/mL	17 fg/mL	[103]
Amperometry	CEA	MoS <sub>2</sub> NFs/Au@AgPt YNCs -Ab2/CEA/Ab1/AuTNP/GCE	10 fg/mL–100 ng/mL	3.09 fg/mL	[87]
EIS	CML	pDNA/PANI-MoS <sub>2</sub> /ITO	10 <sup>-17</sup> –10 <sup>-6</sup> M	3 × 10 <sup>-18</sup> M	[104]
EIS	AFP	Ab/MoS <sub>2</sub> /PDDA/Ag/AgCl wire	0.1–10 ng/mL	0.033 ng/mL	[90]
EIS	miRNA-21	cDNA/pd-MoS <sub>2</sub> @β-FeOOH/Au	1 fM–5 nM	0.11 fM	[88]
EIS	TNF-α	MoS <sub>2</sub> NFs	0.01–200 pg/ml	0.202 pg/ml	[89]
PEC	CEA	ALP-Au-Ab2/CEA /Ab1/ZnS/C/MoS <sub>2</sub> /GCE	2.0 pg/mL–10.0 ng/mL	1.30 pg/mL	[92]
PEC	SCCA	Ab/AuNPs/C/MoS <sub>2</sub> /GCE	0.005–8 ng/mL	1.8 pg/mL	[105]
PEC	AFP	DNA/Au/GaN	1.0–150 ng/mL	0.3 ng/mL	[91]
PEC	MCF-7 cells	PM6:Y6/anti-EpCAM-MNs /Au NPs/Au-aptamer	10–10,000 cell/mL	9 cell/mL	[106]

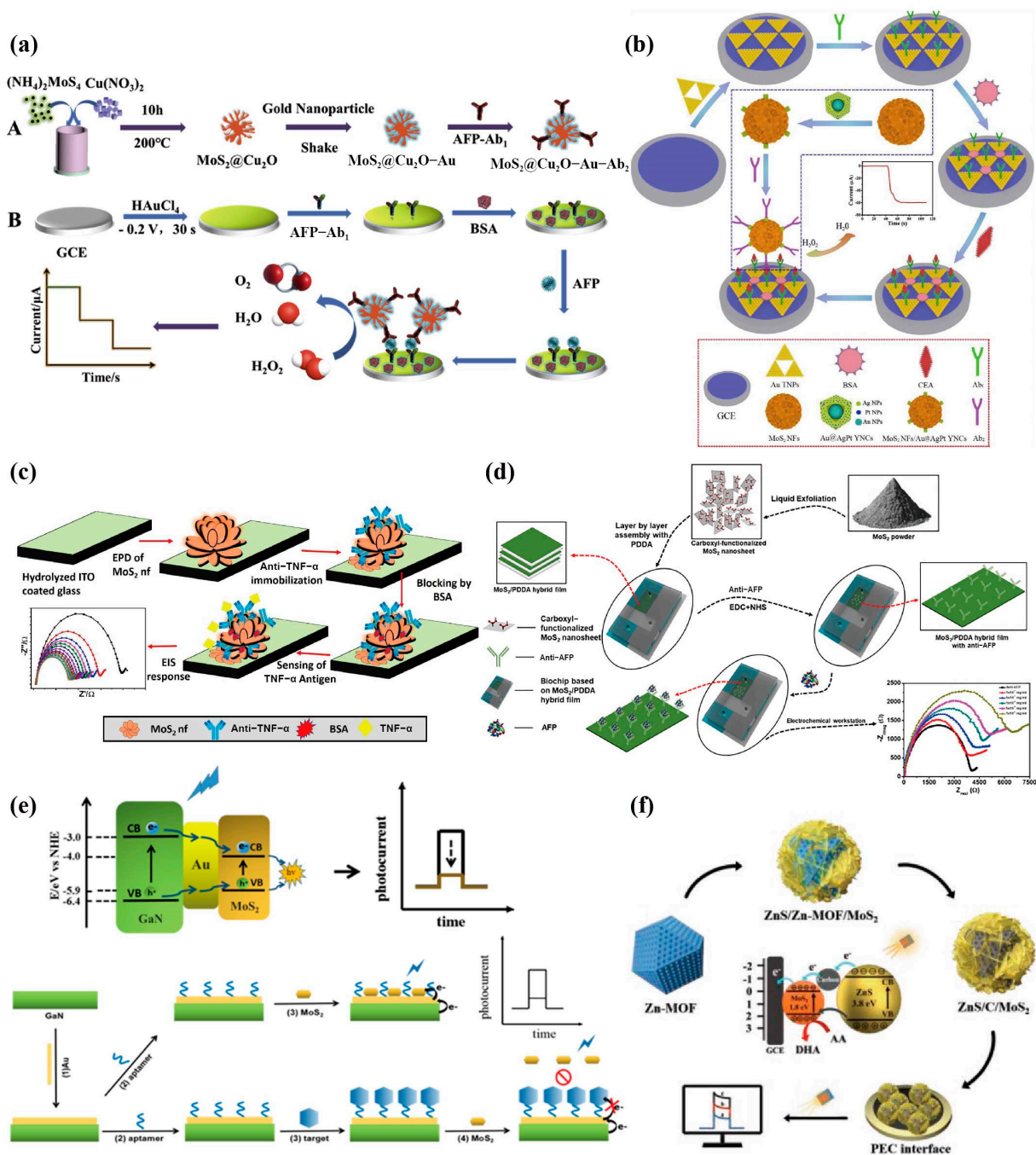


**Figure 4.** Examples of amperometric/impedance/PEC sensors used for detecting various cancer biomarkers. (a) Schematic diagram of ultrasensitive electrochemical immunosensor for AFP detection based on  $\text{MoS}_2@Cu_2O-Au$  [86]. Copyright 2019, Elsevier. (b) Schematic illustration of electrochemical immunosensor based on  $\text{MoS}_2$  NFs/Au@AgPt YNCs as the signal amplification label for sensitive detection of CEA [87]. Copyright 2019, Elsevier. (c) Schematic representation of BSA/anti-TNF- $\alpha$ /MoS<sub>2</sub> NFs/ITO immunoelectrode fabrication [89]. Copyright 2022, Elsevier. (d) Schematic illustration for self-assembly of MoS<sub>2</sub>/PDDA hybrid film, microfluidic chip fabrication, anti-AFP immobilization, and electrochemical detection of AFP [90]. Copyright 2020, Elsevier. (e) Charge-transfer mechanism in MoS<sub>2</sub>/Au/GaN and the AFP detection schematic illustration of the PEC sensor [91]. Copyright 2021, American Chemical Society. (f) Schematic illustration of the stepwise fabrication of ZnS/C/MoS<sub>2</sub> nanocomposite and the enhancement effect on the photocurrent response [92]. Copyright 2019, Wiley.

#### 4. Optical Biosensors for Cancer Biomarker Detection Based on MoS<sub>2</sub>

Optical biosensors bring additional advantages in the fields of biotechnology, environmental research, disease diagnosis, and medical applications due to their high selectivity, and fast and sensitive measurement. The working principle and key performance indicators of optical biosensors largely depend on optical transducers tightly integrated with biological sensing components [107]. Based on different biosensor elements, optical biosensors are divided into colorimetry, electrochemiluminescence (ECL), fluorescence, surface enhanced Raman scattering (SERS), surface plasmon resonance (SPR), and other sensing methods. In combination with MoS<sub>2</sub>, the latest application progress in cancer biomarker detection is introduced.

##### 4.1. Colorimetry

MoS<sub>2</sub>, with its large surface area and exposed reaction sites, can be used as a nano enzyme to show the catalytic activity and excellent stability of peroxidase, and it simulates natural enzymes to make the substrate colour change. This feature is used to build a colorimetric sensor to detect cancer biomarkers [108,109]. Zhao et al. [110] introduced an aptamer to enhance the catalytic activity of MoS<sub>2</sub> NSs on peroxidase substrates and designed a colorimetric sensor for the intuitive detection of CEA, achieving sensitivity detection of CEA by successfully recording absorbance (Figure 5a). The sensor exhibited a linear response in the range of 50 to 1000 ng/mL, with an LOD of 50 ng/mL, demonstrating good specificity and practical application capabilities. Shao et al. [111] utilized the high catalytic activity of MoS<sub>2</sub>-AuNPs nanohybrids to reduce NaBH<sub>4</sub> to 4-NP and make the yellow solution colourless, and constructed a colorimetric immunosensor for CEA detection (Figure 5b). The absorbance peak intensity of the colorimetric sensor maintained a good linear relationship in the range of 5 pg/mL to 10 ng/mL, with an LOD as low as 0.5 pg/mL. Wang et al. [112] developed a new colorimetric nano biological platform for the efficient and highly sensitive capture of circulating tumour cells (CTC), in which the MoS<sub>2</sub> NSs surface was modified with two kinds of aptamer functionalized PH sensitive heterochromatic dyes used as a visual detection chip, which had a good PH sensitivity and high dyeing ability.

##### 4.2. Electrochemiluminescence (ECL)

ECL is a special form of chemiluminescence caused by the redox between electro-generated high-energy radicals [113]. It does not rely on external light excitation and avoids the adverse effects of self-luminous and light scattering [114]. Therefore, it has the characteristics of a precise response, easy control, low noise background signal, high sensitivity, good repeatability, and wide linear range, and has become a powerful tool for biomarker detection and clinical diagnosis in recent years [115,116]. MoS<sub>2</sub> can effectively improve the rate of electron transfer, and it is emerging in the construction of ECL sensing platforms for cancer biomarkers [117]. Zhang et al. [118] used ordered mesoporous carbon-MoS<sub>2</sub> (OMC-MoS<sub>2</sub>) as a sensing platform and Cu<sub>2</sub>O@OMC-Ru (bpy)<sub>3</sub><sup>2+</sup> as signal tags to develop a sandwich ECL immunosensor for the detection of AFP (Figure 5c). As we know, MoS<sub>2</sub> NSs are easy to agglomerate, resulting in a loss of activity, and the synergistic effect of nanocomposites can offset this loss of activity. OMC exhibits an excellent electrocatalytic performance due to its ordered pore structure, high specific surface area, and high porosity [119]. Therefore, OMC-MoS<sub>2</sub> can synergistically increase the effective surface area and conductivity to improve sensor sensitivity. The ECL detection range of AFP is 0.1 pg/mL–10 ng/mL, with an LOD of 0.011 pg/mL (S/N = 3). Liu et al. [120] synthesized MoS<sub>2</sub> NSs using the hydrothermal method, enhanced the electrochemiluminescence signal of sulphur doped boron nitrogen quantum dots (QDs) using its strong surface plasmon coupling (SPC) light absorption effect in visible and near-infrared regions, and constructed an ECL sensing platform amplified by the hybrid chain reaction (HCR) for hepatitis C virus (HCV) genetic testing (Figure 5d).

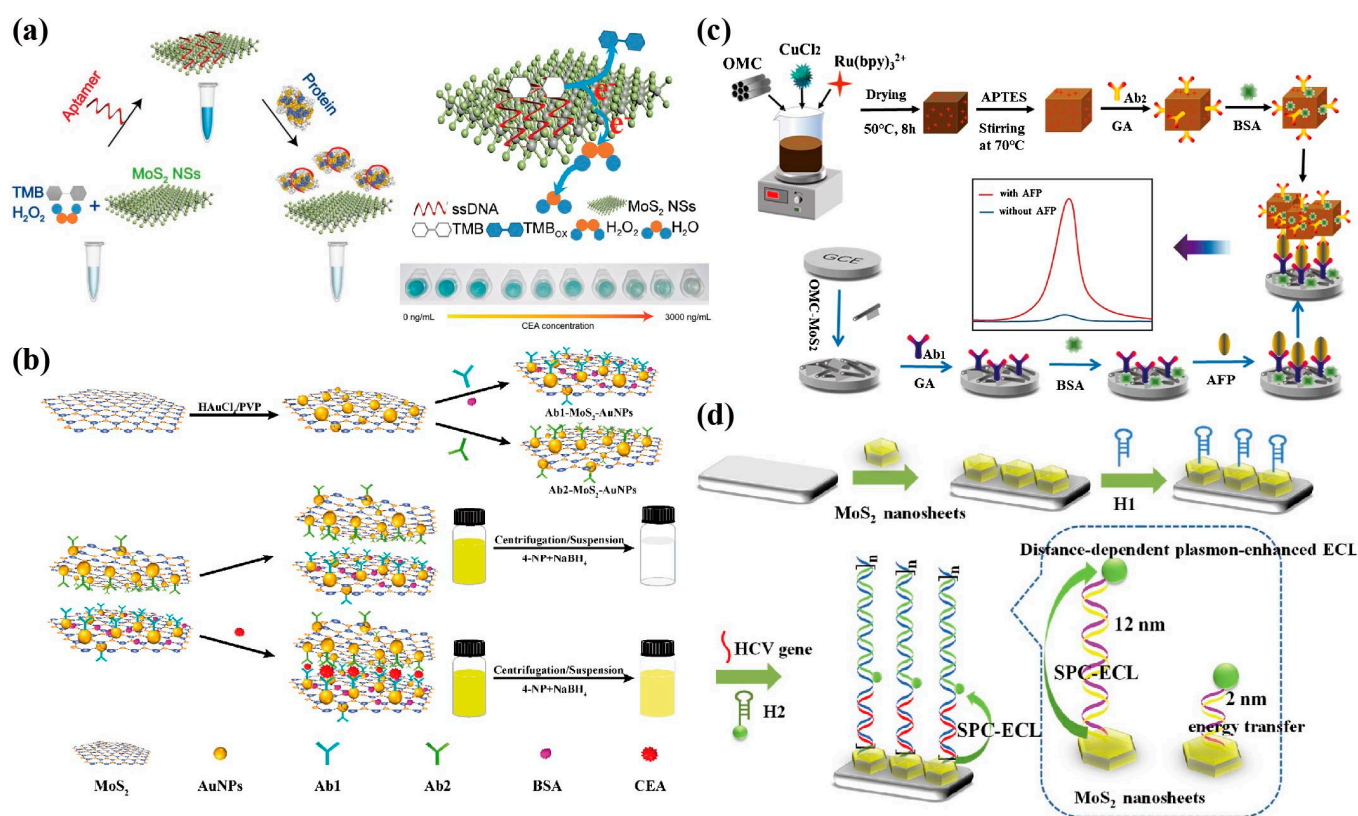


**Figure 5.** Examples of colorimetric/ECL sensors used for detecting various cancer biomarkers. (a) Schematic illustration of the colorimetric biosensor based on aptamer-modified MoS<sub>2</sub> NSs for CEA protein detection [110]. Copyright 2020, RSC Pub. (b) Preparation of MoS<sub>2</sub>-AuNPs nanohybrids and Ab-MoS<sub>2</sub>-AuNPs nanoprobe, and schematic illustration of the colorimetric sensor for CEA detection [111]. Copyright 2019, American Chemical Society. (c) Schematic illustration of the sandwich-configuration ECL immunoassay based on Cu<sub>2</sub>O@OMC-Ru(bpy)<sub>3</sub><sup>2+</sup> and OMC-MoS<sub>2</sub> for the determination of AFP [118]. Copyright 2020, Springer Nature. (d) The HCR-based sensing process and distance-dependent plasmon-enhanced ECL for HCV detection [120]. Copyright 2020, Elsevier.

#### 4.3. Fluorescence

Fluorescence analysis is an advanced analytical method with a high sensitivity, selectivity, and practicality, which can qualitatively and quantitatively analyse the changes in fluorescence intensity, emission spectrum, and fluorescence molecular lifetime of substances [121]. Due to the strong adsorption capacity and wide absorption spectrum of MoS<sub>2</sub> NSs to ssDNA, MoS<sub>2</sub> NSs can quench fluorescent groups with different emission wavelengths, showing unique advantages in the construction of fluorescent biosensor platforms [122]. Liang et al. [123] built a fluorescence sensing platform for the hepatocellular carcinoma (HCC) biomarker GP73 based on the Förster resonance energy transfer (FRET). Among them, utilizing the synergistic effect of the MoS<sub>2</sub>@rGO composites as a fluorescence receptor further enhanced the quenching effect, and the nitrogen-doped graphene QDs modified by the GP73 aptamer were used as fluorescence donors. The detection range was 5 ng/mL to 100 ng/mL, and the LOD was 4.54 ng/mL (S/N = 3). It also showed a good detection effect in human serum. Wang et al. [124] designed QD molecular beacons (QD-MBs) functionalized with a MoS<sub>2</sub> fluorescent probe (QD-MB@MoS<sub>2</sub>) for the dual detection of two kinds of miRNAs related to multiple myeloma (MM), with an LOD as low as the fM level, realizing ultra-high sensitivity detection (Figure 6a). In addition, when the MoS<sub>2</sub> crystal becomes very thin, the transition from the indirect bandgap to the direct bandgap will produce a strong fluorescence [125]. MoS<sub>2</sub> QDs have strong quantum confinement and edge effects and other photoelectric properties, and are widely used in fluorescence sensing,

catalysis, biological imaging, and other fields [126]. Ge et al., based on the quenching of MoS<sub>2</sub> QDs by the inner filter effect (IFE) and rolling circle amplification (RCA) technology, constructed a label-free and highly sensitive miRNA fluorescence detection platform with a high selectivity and satisfactory recovery [126].

#### 4.4. Surface Enhanced Raman Scattering (SERS)

SERS technology can provide molecular fingerprint information, has a high sensitivity and specificity, and does not cause damage to the sample, and is thus considered as a promising analytical technology in the field of disease analysis [127]. SERS sensor composition mainly include substrates, target detection substances, and SERS capture probes. MoS<sub>2</sub> has been applied in the preparation of SERS capture probes due to its large specific surface area, stability, and excellent catalytic performance. Engine et al. [128] developed a SERS sandwich immunosensor for the ultra-sensitive detection of AFP (Figure 6b). Among them, MoS<sub>2</sub> is modified by the monoclonal antibody as the capture probe of AFP, and its high surface area and adsorption capacity for biomolecules make the sensing interface more stable. The SERS immunosensor based on Au@AgNCs/MoS<sub>2</sub> nanocomposites has a good linear response in the range of 1 pg/mL to 10 ng/mL, with an LOD as low as 0.03 pg/mL. Pan et al. [129] developed a sensitive and direct SERS aptasensor for detecting gastric cancer exosomes. AuNSs-decorated MoS<sub>2</sub> NSs (MoS<sub>2</sub>-AuNSs) surfaces were assembled with ROX-labelled aptamers (ROX-Apt) used as nano probes to achieve the ultra-sensitive capture of exosomes (Figure 6c). This sensor quantitatively detected gastric cancer exosomes over a wide range of SERS signals ( $55\text{--}5.5 \times 10^5$  particles/ $\mu\text{L}$ ), with an LOD as low as 17 particles/ $\mu\text{L}$ , which provides a prospective platform for the early diagnosis of gastric cancer. In addition, Hilal et al. [130] developed a sandwich-type SERS immunosensor for the sensitive detection of CEA, which has a good selectivity and stability and is well applied in clinic.

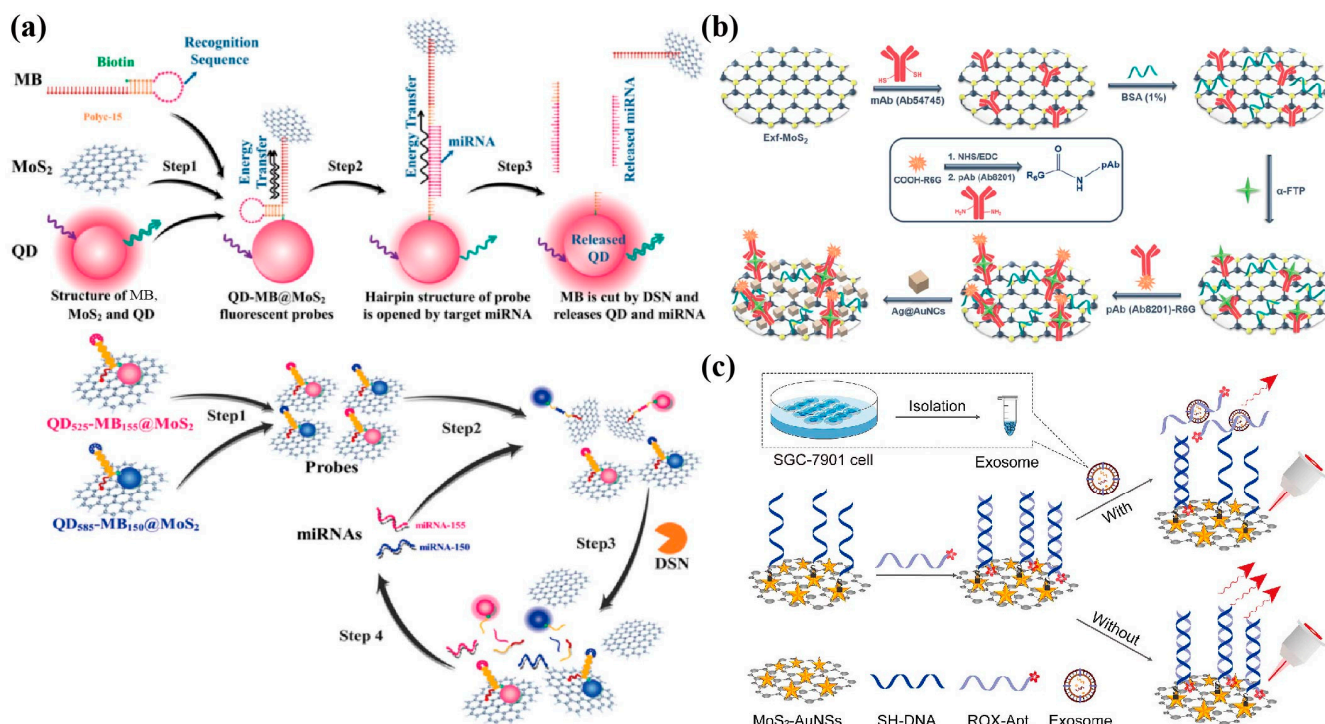


**Figure 6.** Examples of fluorescence/SERS sensors used for detecting various cancer biomarkers. (a) Schematic illustration of dual miRNA detection by QD-MB@MoS<sub>2</sub> fluorescent probes [124]. Copyright 2022, Elsevier. (b) Schematic illustration of the SERS immunosensor based on Au@AgNCs/MoS<sub>2</sub> nanocomposites [128]. Copyright 2021, American Chemical Society. (c) Fabrication of MoS<sub>2</sub>-based aptasensor for exosomes detection [129]. Copyright 2022, Elsevier.

#### 4.5. Surface Plasmon Resonance (SPR)

SPR provides a non-invasive and label-free method to detect analytes. MoS<sub>2</sub> has a large absorption coefficient and high refractive index at 500 nm, whose structure is conducive to the propagation of the surface plasma. Such photoelectric characteristics enhance SPR signals and improve the sensitivity of the sensor [131]. Therefore, the modification of MoS<sub>2</sub> is also applied in SPR sensors for cancer biomarker detection. Chiu et al. [132] prepared MoS<sub>2</sub> by the liquid-phase exfoliation and covalently functionalized it to form carboxyl-functionalized MoS<sub>2</sub> (carboxyl-MoS<sub>2</sub>) acting as a signal amplification sensing modification layer. The carboxylation modification effectively improved the sensitivity of the SPR sensor. The SPR chip based on carboxyl-MoS<sub>2</sub> was used to specifically detect the lung cancer-associated biomarker cytokeratin 19 fragment (CYFRA21-1), which shows a wide linear range (0.05 pg/mL–100 ng/mL) and low LOD (0.05 pg/mL), and has a good specificity, selectivity, sensitivity, and affinity. Compared with traditional SPR bare gold chips, the SPR chip has many characteristics, such as a unique glycan matrix structure, high surface area carboxylic acid groups, and excellent biological affinity. In addition to the above sensing methods, other sensing methods based on MoS<sub>2</sub> are listed in the Table 2 to detect various cancer biomarkers.

**Table 2.** Optical biosensors for cancer biomarker detection based on MoS<sub>2</sub>.

Method	Analytes	Electrode/Label	Linear Range	LOD	Ref.
Colorimetry	CEA	Au NPs-MoS <sub>2</sub> -Ab2/ CEA/Ab1/MoS <sub>2</sub> -Au NPs	5 pg/mL–10 ng/mL	0.5 pg/mL	[111]
Colorimetry	CEA	DNA/MoS <sub>2</sub> NSs	50–1000 ng/mL	50 ng/mL	[110]
Colorimetry	CTC	TP/SYL <sub>3</sub> C-MoS <sub>2</sub>	5–10 <sup>4</sup> cells/mL	2 cells/mL	[112]
ECL	CEA	Ab/MOF-545-Zn@MQDs/GCE	0.18–1000 ng/mL	0.45 pg/mL	[133]
ECL	PSA	GOD-SiO <sub>2</sub> -Ab2/PSA /Ab1/MoS <sub>2</sub> -AuNPs/GCE	0.5 pg/mL–10.0 ng/mL	0.20 pg/mL	[134]
ECL	HCV gene	S-BN QDs-hairpin DNA2 (H2)/MoS <sub>2</sub> Ns	0.5 pmoL/L–1 nmoL/L	0.17 pmoL/L.	[121]
ECL	HPV 16 DNA	Zn-doped MoS <sub>2</sub> QDs & QD-DNA/reductive Cu(I) particles	0.1–200 nmolL	0.03 nmol/L	[135]
ECL	miRNA-210	S dots/Au NP@MoS <sub>2</sub> NSs	0.1 pM–10 nM	0.03 pM	[136]
ECL	miRNA-21	luminophore/MoS <sub>2</sub> QDs@Zeolitic Imidazolate 2 Framework-8	Buffer (0.1 mM PBS), co-reactant (2 mM H <sub>2</sub> O)	14.6 aM	[137]
Fluorescence	CA15-3	DNA/MoS <sub>2</sub> NSs	0.01–0.1 U/mL	0.0039 U/mL	[138]
Fluorescence	PD-1	MoS <sub>2</sub> -NFP	125–8000 pg/mL	85.5 pg/mL	[139]
Fluorescence	miRNA-155 & miRNA-150	QD-MB @MoS <sub>2</sub>	10 fM–1 nM	7.19 fM & 5.84 fM	[124]
SERS	CEA	MoS <sub>2</sub> NFs@Au NPs/MBA-Ab2/CEA /Ab1/Fe <sub>3</sub> O <sub>4</sub> NPs@Au NPs/ d-Ti <sub>3</sub> C <sub>2</sub> TX Mxene	0.0001–100.0 ng/mL	0.033 pg/mL	[132]
SERS	CA19-9	R6G-tagged MoS <sub>2</sub> NF	5 × 10 <sup>-3</sup> –100 IU/mL	3.43 × 10 <sup>-4</sup> IU/mL	[140]
SERS	exosomes	MoS <sub>2</sub> -AuNSs/ROX-Apt	55–5.5 × 10 <sup>5</sup> particles/μL	17 particles/μL	[131]
SPR	CYFRA21-1	Ab/COOH-MoS <sub>2</sub> /Au/Cr/BK7	0.05 pg/mL–100 ng/mL	0.05 pg/mL	[132]

#### 5. Miscellaneous Biosensors for Cancer Biomarkers Detection Based on MoS<sub>2</sub>

In addition to the two main types of cancer biomarker sensing platforms based on optics and electrochemistry, this section covers some other types of cancer biomarker sensors based on MoS<sub>2</sub>. MoS<sub>2</sub> has the characteristics of a direct bandgap, excellent switching ratio, and high carrier mobility [141], which makes the MoS<sub>2</sub> field effect transistor (FET) biosensor have the advantages of a high sensitivity, label-free biological detection, system integration, and easy manufacturing. Recently, Shi et al. [142] used 2D carbon-coated MoS<sub>2</sub> NRs to form an overlapping hybrid structure (MoS<sub>2</sub>@C), combined with HCR, 3D DNA walker, and DNA hexahedron nano framework, which established a novel four-fold amplification and self-powered intelligent sensing platform for the ultra-sensitive colorimetric/electrochemical dual-mode detection of tumour suppressor miRNAs in HCC

(Figure 7a). As a hollow network structure, MoS<sub>2</sub>@C can extend the interlayer distance, not only improving the stability of the materials, but also providing more enzymes and probe binding sites. This sensor quantifies the concentration of miRNAs by measuring the open circuit voltage and colour changes of MBs, making it an efficient, sensitive, and highly specific sensing method. Wang et al. [143] mixed metals and semiconductors to make MoS<sub>2</sub> composite (1T-MoS<sub>2</sub>) as an excellent substrate with a high conductivity and electronic density of state, and combined it with the 2D graphitic carbon nitride (g-C<sub>3</sub>N<sub>4</sub>) to build a recyclable immunoassay platform for CA125 (Figure 7b), with an LOD as low as  $4.96 \times 10^{-4}$  IU/mL. Based on the excellent electronic properties and high specific recognition ability of MoS<sub>2</sub> NSs, Yang et al. [144] constructed a FET sensor array to detect the bladder cancer biomarkers nuclear matrix protein 22 (NMP22) and cytokeratin 8 (CK8), and achieved ultra-sensitive detection in a wide linear range ( $10^{-6}$ – $10^{-1}$  pg/mL), with an LOD as low as 0.027 aM and 0.019 aM (Figure 7c). Zhang et al. [145] functionalized MoS<sub>2</sub> FET by coupling DNA tetrahedron and biotin-streptavidin, and detected PSA in the range of 1 fg/mL–100 ng/mL, with broad development prospects in the field of real-time detection (Figure 7d).

In recent years, aptasensors have become a major class of sensor technology. Aptamers are single stranded nucleotides (ssDNA or ssRNA) synthesized through systematic evolution of ligands by exponential enrichment (SELEX). With different sequences and 3D structures, they can specifically bind to various targets, such as small molecules, proteins, whole cells, and nucleotide sequences [146]. Aptamers are “chemical antibodies” that detect analytes based on conformational changes, which have the advantages of a small size, high chemical stability, high specificity, easy synthesis and modification, and low cost, etc., and which are widely used in the field of novel biosensing technologies in combination with numerous nanomaterials. Shi et al. [147] constructed a biofuel cell based on a hybridization chain reaction and catalytic hairpin assembly (CHA) self-assembly, and developed an electrochemical/colorimetric dual mode biosensing platform for identifying the colon cancer inhibitory factor miRNA-199a (Figure 8a–c). The bioanode of this biofuel cell is a flexible carbon cloth loaded with glucose oxidized-functionalized MoS<sub>2</sub> NRs, and the bio-cathode is composed of double stranded deoxyribonucleotide chains generated by nucleic acid amplification technology. The combination of high surface area MoS<sub>2</sub> NRs, enzyme-free cascade signal amplification technology, and non-interference dual mode detection strategy makes the sensor highly sensitive, selective, and accurate. The sensor has an electrochemical linear range of 0.1 fM–100 pM, LOD of 24.1 aM (S/N = 3), colorimetric linear range of 0.1 fM–10,000 pM, and LOD of 34.5 aM (S/N = 3), is a promising method for detecting colorectal cancer inhibitory factors. Similarly, Hou et al. [148] also developed a self-powered biosensor based on ultrasensitive enzyme biofuel cell in the same year for electrochemical/colorimetric dual mode detection of HER2 (Figure 8d–g). The selected construction materials for this biofuel cell were 1T-MoS<sub>2</sub> and graphdiyne, among which 1T-MoS<sub>2</sub> is a metal phase of MoS<sub>2</sub>, which has an extraordinary conductivity, enlarged interlayer spacing, and abundant reaction sites, greatly improving the performance of the battery. Furthermore, Lee et al. [149] developed a DNA aptamer/MoS<sub>2</sub> heterolayer electrobiosensor and achieved ultra-sensitive early diagnosis of exosomes combined with an interdigitated microgap electrode (IDMGE) system (Figure 8h). MoS<sub>2</sub> nanoparticles have a good biomolecular detection ability, more effectively immobilizing the aptamer and improving the electrical sensitivity of the sensor. Based on the work function tuning strategy, Hou et al. [136] constructed an AuNPs@MoS<sub>2</sub> NSs heterostructure with a large specific surface area, good biocompatibility, good electrocatalytic activity, and high conductivity, and developed a new ECL sensor for the detection of miRNA-210 in triple negative breast cancer tissues (Figure 8i,j). Due to the small bandgap of MoS<sub>2</sub> NSs, the ECL quenching ability of AuNPs by close range electron transfer can be effectively suppressed in the heterostructure, while also improving the conductivity and LSPR performance of AuNPs. In addition to the above sensing methods, other sensing methods for detecting various cancer biomarkers based on MoS<sub>2</sub> are listed in Table 3.

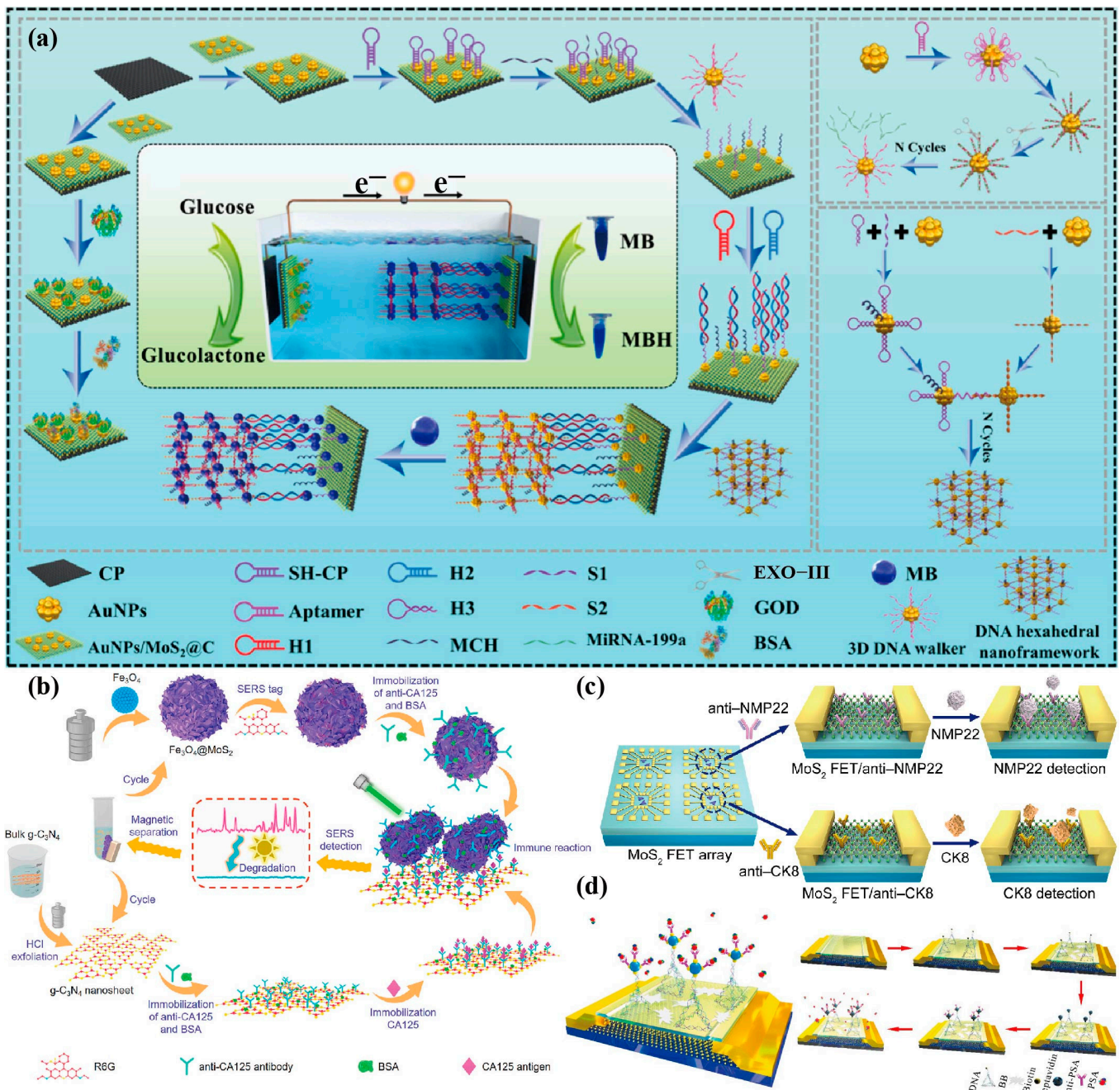


**Figure 7.** (a) Creation of an ultra-sensitive dual-mode approach based on self-powered sensor detecting liver cancer makers [142]. Copyright 2023, Elsevier. (b) Fabrication of Fe<sub>3</sub>O<sub>4</sub>@MoS<sub>2</sub> composites and g-C<sub>3</sub>N<sub>4</sub> NSs as well as the protocol of recyclable SERS-based sandwich immunoassay [143]. Copyright 2023, Elsevier. (c) Schematic illustration of MoS<sub>2</sub> NSs-based FET sensor array for the simultaneous detection of NMP22 and CK8 [144]. Copyright 2020, Springer Nature. (d) Surface functionalization and electrical characterization of the MoS<sub>2</sub> FET device. Schematic diagram showing the 3D structure of the functionalized MoS<sub>2</sub> biosensor (left plate). Flow chart of the device functionalization process (right plate) [145]. Copyright 2021, Elsevier.

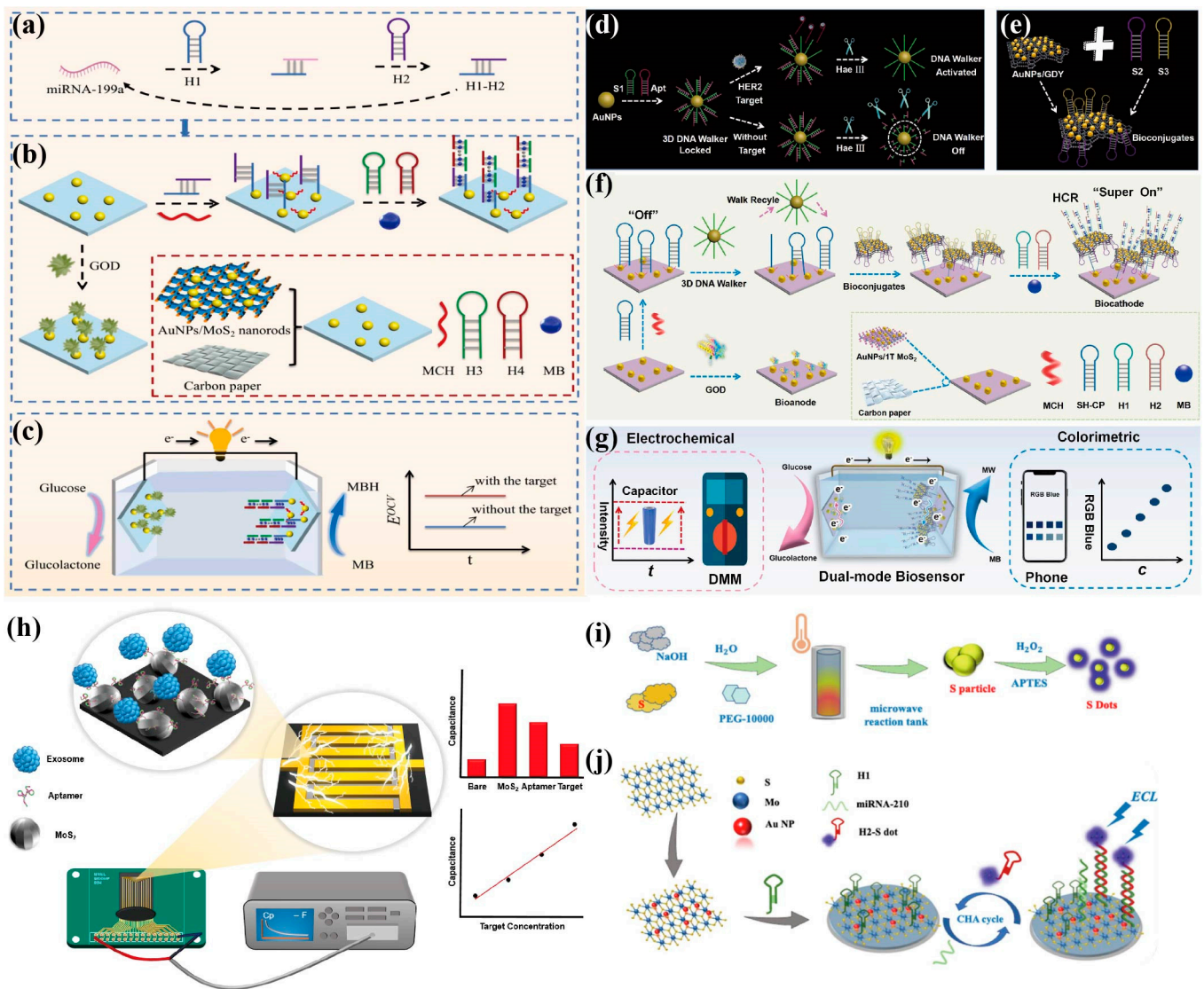


**Figure 8.** Detail diagram of the preparation process of the self-powered biomolecular sensing system [147]. (a) The CHA process involving the target object. (b) The establishment process of the bioanode and bio-cathode. (c) Schematic representation of the assembly of the self-powered biosensor. Copyright 2023, Elsevier. Schematic illustration of dual-mode self-powered biosensing platform [148]. (d) HER2 recognition activates 3D DNA walker. (e) Preparation of bioconjugates. (f) Assembly process of biological electrodes. (g) The detection mechanism of the dual-mode strategy. Copyright 2023, Elsevier. (h) Schematic image of an exosome detection biosensor [149]. Copyright 2022, Elsevier. Illustration of (i) the synthesis of S dots and (j) the ECL sensing system based on S dots and Au NP@MoS<sub>2</sub> nanosheet heterostructure [136]. Copyright 2022, Elsevier.

**Table 3.** Miscellaneous biosensors for cancer biomarkers detection based on MoS<sub>2</sub>.

Method	Analytes	Electrode/Label	Linear Range	LOD	Ref.
FET array	NMP22 & CK8	MoS <sub>2</sub> NSs-FET	10 <sup>-6</sup> –10 <sup>-1</sup> pg/mL	0.027–0.019 aM	[144]
DeMEA/ microfluidic	exosome	GASI microfluidic channel/anti-EpCAM	1 × 10 <sup>2</sup> –1 × 10 <sup>9</sup> exosomes/μL	17 exosomes/μL	[150]
EIS/CV	T <sub>3</sub>	Au-MoS <sub>2</sub> /anti-T <sub>3</sub> electrodes	0.01–100 ng/mL	2.5 pg/mL	[151]
SAW	CEA	AuNP–MoS <sub>2</sub> -rGO/PI	0.1–80 ng/mL	0.084 ng/mL	[152]
bio-FET	PSA	MoS <sub>2</sub> /B-SA system with DNA tetrahedron	1 fg/mL–100 ng/mL (PBS) 1 fg/mL–100 ng/mL (serum)	1 fg/mL	[145]
Paper-Based/DPV	miRNA-1	AuNPs/RGO/PE	33.8–135.3 nM	12.0 nM	[153]
	55miRNA-21	AuNPs/MoS <sub>2</sub> /PE	135.6–406.8 nM	25.7 nM	
Microfluidic/ electrochemical/visual signal amplification/ 3D DNA walker	miRNA-141	Bi <sub>2</sub> S <sub>3</sub> @MoS <sub>2</sub> NFs/CeO <sub>2</sub>	10 fM–1 nM 0.5 fM–1 nM	0.12 fM 2.65 fM	[154]
SERS/ELISA	microRNA-199a	AuNPs/MoS <sub>2</sub> @C	0.0001–100 pM	4.94 amol/L	[142]
SERS/ELISA	ferritin	MoS <sub>2</sub> @Fe <sub>3</sub> O <sub>4</sub> /BP	10–10 <sup>-4</sup> μg/mL	7.3 × 10 <sup>-5</sup> μg/mL	[155]
colorimetric/ electrochemical dual mode	CA125	Fe <sub>3</sub> O <sub>4</sub> @MoS <sub>2</sub> /g-C <sub>3</sub> N <sub>4</sub> NSs	10 <sup>-3</sup> –10 <sup>2</sup> IU/mL	4.96 × 10 <sup>-4</sup> IU/mL	[143]
colorimetric/ electrochemical dual mode	miRNA-199a	MoS <sub>2</sub> NRs/CHA /HCR/MB	0.1–10 <sup>5</sup> fM & 0.1–10 <sup>7</sup> fM	0.0241 aM & 0.0345 aM	[147]
capacitance electrochemical dual mode	HER2	3D DNA walker /1T-MoS <sub>2</sub> /graphdiyne	0.0001–10 pg/mL	0.03 pg/mL	[148]
ECL/LSPR	exosome	MoS <sub>2</sub> heterolayer/ IDMGE	10 <sup>4</sup> –10 <sup>8</sup> exosomes/mL	2192.6 exosomes/mL	[149]
electrochemistry	miRNA-210	S dots/AuNPs@MoS <sub>2</sub> NSs heterostructure	0.1 pM–10 nM	0.03 pM	[136]
ECL/CHA	PSA	MoS <sub>2</sub> /SiO <sub>2</sub> NPs	1 fg/mL–500 ng/mL	2.5 fg/mL	[156]
LSAW aptasensor	miRNA-210	MoS <sub>2</sub> NSs@biomimetic magnetic vesicles	1 fM–100 pM	0.3 fM	[157]
PEC/EIS	AFP	monolayer MoS <sub>2</sub> /Au NPs/aaptamer	0.01–100 ng/mL	4.79 pg/mL	[158]
EIS/microscopic	miR-92a-3p	MoS <sub>2</sub> @Ti <sub>3</sub> C <sub>2</sub>	1–10 <sup>8</sup> fM	0.27 fM	[159]
FET	OFA/iLRP	AB3/GO/SPE	10–300 k cells/mL	16 cells/mL	[160]
Fluorescence/ ECL	BRCA1	Ag-Au@Ins/Apta-MIP without template modified Au gate MoS <sub>2</sub> FET	10 aM–1.0 nM	6.4 aM	[161]
	miRNA-21	carbon dots	0.1 pM–1 nM	21.1 fM	[162]
	miRNA-135b	MoS <sub>2</sub> QDs	30 fM–20 nM	10 fM	

## 6. Discussion and Outlook

As a representative of TMDs, the unique bandgap adjustable layered structure of MoS<sub>2</sub> has shown excellent optical, electronic, and mechanical properties in the construction of sensing interfaces, and has further expanded the application of MoS<sub>2</sub> as a sensing electrode in different functionalization processes. It is a promising nanomaterial to replace GO and other semiconductor devices. According to the above, the composite-based sensing interfaces built on MoS<sub>2</sub> have been widely used in the detection of different cancer biomarkers. These sensing platforms have shown a good sensitivity, specificity, and reproducibility, comprehensively proving the great potential of MoS<sub>2</sub> in early cancer screening. However, MoS<sub>2</sub> still faces severe challenges and further development.

As the growth process of MoS<sub>2</sub> is uncontrollable, how to reduce the influence of impurities and lattice defects and find a large-scale and high-quality synthesis method are the fundamental issues of MoS<sub>2</sub>. Two-dimensional MoS<sub>2</sub> has the defect of easy aggregation, which leads to a reduction in electrochemical activity. Accurate control of the synthesis of MoS<sub>2</sub> with a uniform thickness, ideal size, and colloidal stability still needs further exploration. Although these shortages can be improved by modifying MoS<sub>2</sub> with molecules, nanoparticles, or single-atom sites to form composites, achieving controllable parameters such as shape, size, charge, stability, and surface chemistry during the design process remains a major challenge [163]. Therefore, advanced synthesis techniques are needed to address these issues, such as exploring surface constrained synthesis methods and exploring better exfoliative conditions using material informatics prediction methods [164]. The covalent/non-covalent functionalization of MoS<sub>2</sub> is a powerful tool to improve the dispersion and stability, and to effectively expand its application by adjusting the physical properties or adding new attributes [78]. For example, changing the MoS<sub>2</sub> ratio of 2H and 1T crystal structures by inducing defects or introducing additional negative charges, as well as changing the MoS<sub>2</sub> bandgap through doping, embedding, and other methods [41]. By using these approaches, MoS<sub>2</sub> can be promoted to achieve low-cost, reliable, and large-scale production, which will effectively expand the construction and application capabilities of

composite-based sensing interfaces based on MoS<sub>2</sub>. These new developments will drive different composite-based sensing interfaces based on MoS<sub>2</sub> into a new era.

The conversion of MoS<sub>2</sub> between different dimensions makes its characteristics and applications rich, for example as semiconductor, metal, or superconducting materials. For example, 2H-MoS<sub>2</sub> and 3R-MoS<sub>2</sub> can be used for dry lubricating oil [75]. The nonlinear optical properties of 3R-MoS<sub>2</sub> can be used for quantum measurements and nonlinear optical quality sensing in the biomedical field. Although MoS<sub>2</sub> shows good electronic properties, compared with silicon, its electron mobility is lower and its bandgap is higher, which still creates many problems in the construction of MoS<sub>2</sub> FET sensors. The conductivity of MoS<sub>2</sub> NSs is affected by temperature and thickness, which increases with increasing temperature and decreases with increasing thickness until it reaches a 3D structure [76]. Furthermore, MoS<sub>2</sub> also has good characteristics of electron-spin and magnetoresistance. The research shows that MoS<sub>2</sub> has half-metallic ferromagnetism when doped with Sc, and has a unified spin-polarization value, which is conducive to the development of spintronics [77]. The key factor for the wide application of MoS<sub>2</sub> in optoelectronics is that it has an adjustable bandgap that changes with size and structure. The change in the bandgap dimension leads to a change in photoluminescence characteristics. MoS<sub>2</sub> QDs have a higher bandgap than MoS<sub>2</sub> NSs, whose optical properties can be changed by adjusting the size, or the photoluminescence intensity, and the emission rate can be enhanced according to the light–matter interaction. MoS<sub>2</sub> can realize broadband detection from visible light to far infrared, which is of great significance for safety, biosensors, and thermal imaging, but its responsivity and detection rate are poor due to poor light absorption and large dark current [165]. We also found that the quenching ability of MoS<sub>2</sub> is easily affected by water and oxygen in the medium. Additionally, although MoS<sub>2</sub> has good biocompatibility, bioabsorption, anti-cancer, and antibacterial effects in catalytic and biological activity applications, it also has a high toxicity [166].

In this work, the applications of electrochemical and optical sensing platforms based on MoS<sub>2</sub> in the field of early cancer diagnosis are reviewed. In fact, MoS<sub>2</sub> shines brightly in many fields due to its rich and colourful excellent characteristics. As an example, MoS<sub>2</sub> is a suitable battery electrode material, can be used for hydrogen evolution reactions, has great application prospects in biomedical fields such as cancer treatment and relevant fields of the Internet of Things, and even performs a certain function in emerging technological fields such as microwave and terahertz technology. Furthermore, the miniaturization of the sensing technology is of great significance for point of care testing (POCT). Now, with the popularity of miniaturized electronic devices, wearable, portable devices, electronic skin, and other emerging technologies have been developed rapidly. MoS<sub>2</sub>, with its good mechanical properties, has become the best candidate material for flexible sensors that can be attached to the skin to achieve non-invasive detection of biomarkers in body fluids, thus minimizing skin irritation and making it easy to measure [167]. The detection of cancer biomarkers in sweat and other bodily fluids (such as saliva and urine) based on MoS<sub>2</sub> flexible sensing interfaces needs further development, which cannot be separated from the development of electronic circuits, wireless communication units, and power supply systems.

## 7. Conclusions

In this review, we summarize the application of MoS<sub>2</sub>-based electrochemical and optical sensing platforms in the field of early cancer diagnosis, and explore the improvement and application of the MoS<sub>2</sub> synthesis process and material properties in the construction of biosensor platforms, and focus on the excellent characteristics of MoS<sub>2</sub> and its composite materials in the construction of electrochemical and optical sensing platforms, as well as their applications in the field of cancer biomarkers detection. Nowadays, although MoS<sub>2</sub> still faces significant challenges in synthesis technology, enhancement of dispersion, and conductivity, the interdisciplinary development of materials informatics and other disciplines has led to an increasing number of material synthesis methods being used

for the study of MoS<sub>2</sub>. It has been proven that MoS<sub>2</sub> plays a crucial role in healthcare, optoelectronics, energy, chemical, and mechanical industries.

**Author Contributions:** Z.Q. literature research and collation, conceptualization, methodology, data curation, writing—original draft; J.Z.: information access, writing—revising; S.L.: structural design, writing—review and editing, supervision. All authors have read and agreed to the published version of the manuscript.

**Funding:** This work was supported by the National Key Research and Development Program of China (grant no. 2022YFF1202700), the National Natural Science Foundation of China (grant no. 82001922), and the HongKong Scholars Program (grant no. XJ2021034).

**Institutional Review Board Statement:** Not applicable.

**Informed Consent Statement:** Not applicable.

**Data Availability Statement:** Not applicable.

**Conflicts of Interest:** The authors declare no conflict of interest.

### Abbreviations

AuNPs	gold nanoparticles;
rGO	reduced graphene oxide;
PDDA	poly dimethyl diallyl ammonium chloride;
Ag/AgCl	silver/silver chloride;
ITO	indium tin oxide;
AMACR	alpha-methylacyl-CoA racemase;
NaBH <sub>4</sub>	sodium borohydride;
4-NP	4-nitrophenol;
ssDNA	single strand DNA;
AgNCs	gold nanocubes;
AuNS	gold nanostars;
CTC	circulating tumor cells;
PD-1	programmed cell death protein 1;
CYFRA21-1	cytokeratin 19 fragment (1);
T <sub>3</sub>	triiodothyronine;
DSN	duplex-specific nuclease.
LSAW	Love-mode surface acoustic wave
OFA/iLRP	Oncofetal antigen/immature laminin receptor protein
BRCA1	Breast cancer susceptibility gene type 1

### References

- Jayanthi, V.S.; Das, A.B.; Saxena, U. Recent advances in biosensor development for the detection of cancer biomarkers. *Biosens. Bioelectron.* **2017**, *91*, 15–23. [[CrossRef](#)]
- Hasan, M.R.; Ahommed, M.S.; Daizy, M.; Bacchu, M.S.; Ali, M.R.; Al-Mamun, M.R.; Aly Saad Aly, M.; Khan, M.Z.H.; Hossain, S.I. Recent development in electrochemical biosensors for cancer biomarkers detection. *Biosens. Bioelectron.* **2021**, *8*, 100075. [[CrossRef](#)]
- Rabie, A.M.I.; Ali, A.S.M.; Al-Zeer, M.A.; Barhoum, A.; El-Hallouty, S.; Shousha, W.G.; Berg, J.; Kurreck, J.; Khalil, A.S.G. Spontaneous Formation of 3D Breast Cancer Tissues on Electrospun Chitosan/Poly(ethylene oxide) Nanofibrous Scaffolds. *ACS Omega* **2022**, *7*, 2114–2126. [[CrossRef](#)] [[PubMed](#)]
- Gric, T.; Sokolovski, S.G.; Navolokin, N.; Glushkovskaya, O.S.; Rafailov, E.U. Metamaterial formalism approach for advancing the recognition of glioma areas in brain tissue biopsies. *Opt. Mater. Express* **2020**, *10*, 1607–1615. [[CrossRef](#)]
- Ranjan, R.; Esimbekova, E.N.; Kratasyuk, V.A. Rapid biosensing tools for cancer biomarkers. *Biosens. Bioelectron.* **2017**, *87*, 918–930. [[CrossRef](#)] [[PubMed](#)]
- Henry, N.L.; Hayes, D.F. Cancer biomarkers. *Mol. Oncol.* **2012**, *6*, 140–146. [[CrossRef](#)]
- Khan, H.; Shah, M.R.; Berek, J.; Malik, M.I. Cancer biomarkers and their biosensors: A comprehensive review. *TrAC Trends Anal. Chem.* **2023**, *158*, 116813. [[CrossRef](#)]
- Sharifi, M.; Avadi, M.R.; Attar, F.; Dashtestani, F.; Ghorchian, H.; Rezayat, S.M.; Saboury, A.A.; Falahati, M. Cancer diagnosis using nanomaterials based electrochemical nanobiosensors. *Biosens. Bioelectron.* **2019**, *126*, 773–784. [[CrossRef](#)]

9. Agnolon, V.; Contato, A.; Meneghello, A.; Tagliabue, E.; Toffoli, G.; Gion, M.; Polo, F.; Fabricio, A.S.C. ELISA assay employing epitope-specific monoclonal antibodies to quantify circulating HER2 with potential application in monitoring cancer patients undergoing therapy with trastuzumab. *Sci. Rep.* **2020**, *10*, 3016. [[CrossRef](#)]
10. Dueck, M.E.; Lin, R.; Zayac, A.; Gallagher, S.; Chao, A.K.; Jiang, L.X.; Datwani, S.S.; Hung, P.; Stieglitz, E. Precision cancer monitoring using a novel, fully integrated, microfluidic array partitioning digital PCR platform. *Sci. Rep.* **2019**, *9*, 19606. [[CrossRef](#)]
11. Selvakumar, S.C.; Preethi, K.A.; Ross, K.; Tusubira, D.; Khan, M.W.A.; Mani, P.; Rao, T.N.; Sekar, D. CRISPR/Cas9 and next generation sequencing in the personalized treatment of Cancer. *Mol. Cancer* **2022**, *24*, 83. [[CrossRef](#)] [[PubMed](#)]
12. Udo, R.; Katsumata, K.; Kuwabara, H.; Enomoto, M.; Ishizaki, T.; Sunamura, M.; Nagakawa, Y.; Soya, R.; Sugimoto, M.; Tsuchida, A. Urinary charged metabolite profiling of colorectal cancer using capillary electrophoresis-mass spectrometry. *Sci. Rep.* **2020**, *10*, 21057. [[CrossRef](#)] [[PubMed](#)]
13. Barhoum, A.; Altintas, Z.; Shalini Devi, K.S.; Forster, R.J. Electrochemiluminescence biosensors for detection of cancer biomarkers in biofluids: Principles, opportunities, and challenges. *Nano Today* **2023**, *50*, 101874. [[CrossRef](#)]
14. Ibrahim, J.; Peeters, M.; Camp, G.V.; Beeck, K.O. Methylation biomarkers for early cancer detection and diagnosis: Current and future perspectives. *Eur. J. Cancer* **2023**, *178*, 91–113. [[CrossRef](#)] [[PubMed](#)]
15. Raghavendra, U.; Gudigar, A.; Paul, A.; Goutham, T.S.; Inamdar, M.A.; Hegde, A.; Devi, A.; Ooi, C.P.; Deo, R.C.; Barua, P.D.; et al. Brain tumor detection and screening using artificial intelligence techniques: Current trends and future perspectives. *Comput. Biol. Med.* **2023**, *163*, 107063. [[CrossRef](#)] [[PubMed](#)]
16. Yang, G.; Xiao, Z.; Tang, C.; Deng, Y.; Huang, H.; He, Z. Recent advances in biosensor for detection of lung cancer biomarkers. *Biosens. Bioelectron.* **2019**, *141*, 111416. [[CrossRef](#)]
17. Thévenot, D.R.; Toth, K.; Durst, R.A.; Wilson, G.S. Electrochemical biosensors: Recommended definitions and classification. *Biosens. Bioelectron.* **2001**, *16*, 121–131. [[CrossRef](#)]
18. Choi, S.; Goryll, M.; Sin, L.Y.M.; Wong, P.K.; Chae, J. Microfluidic-based biosensors toward point-of-care detection of nucleic acids and proteins. *Microfluid. Nanofluidics* **2011**, *10*, 231–247. [[CrossRef](#)]
19. Kukkar, M.; Tuteja, S.K.; Sharma, A.L.; Kumar, V.; Paul, A.K.; Kim, K.-H.; Sabherwal, P.; Deep, A. A New Electrolytic Synthesis Method for Few-Layered MoS<sub>2</sub> Nanosheets and Their Robust Biointerfacing with Reduced Antibodies. *ACS Appl. Mater. Interfaces* **2016**, *8*, 16555–16563. [[CrossRef](#)]
20. Turner, A.P. Biosensors: Sense and sensibility. *Chem. Soc. Rev.* **2013**, *42*, 3184–3196. [[CrossRef](#)]
21. Vaddiraju, S.; Legassey, A.; Wang, Y.; Qiang, L.; Burgess, D.J.; Jain, F.; Papadimitrakopoulos, F. Design and fabrication of a high-performance electrochemical glucose sensor. *J. Diabetes Sci. Technol.* **2011**, *5*, 1044–1051. [[CrossRef](#)] [[PubMed](#)]
22. Bozal-Palabiyik, B.; Uslu, B.; Marrazza, G. Chapter 11—Nanosensors in Biomarker Detection. In *New Developments in Nanosensors for Pharmaceutical Analysis*; Academic Press: Cambridge, MA, USA, 2019; pp. 327–380. [[CrossRef](#)]
23. Kausar, M. Pesticidal activity of Pakistani *Bacillus thuringiensis* isolates against *Helicoverpa armigera* (Hubner) and *Earias vittella* (Lepidoptera: Noctuidae). *IOSR J. Pharm. Biol. Sci.* **2013**, *4*, 9–12. [[CrossRef](#)]
24. Kaya, S.I.; Ozcelikay, G.; Mollarasouli, F.; Bakirhan, N.K.; Ozkan, S.A. Recent achievements and challenges on nanomaterial based electrochemical biosensors for the detection of colon and lung cancer biomarkers. *Sens. Actuators B Chem.* **2022**, *351*, 130856. [[CrossRef](#)]
25. Nawz, T.; Safdar, A.; Hussain, M.; Sung Lee, D.; Siyar, M. Graphene to Advanced MoS<sub>2</sub>: A Review of Structure, Synthesis, and Optoelectronic Device Application. *Crystals* **2020**, *10*, 902. [[CrossRef](#)]
26. Zhu, S.; Liu, Y.; Gu, Z.; Zhao, Y. Research trends in biomedical applications of two-dimensional nanomaterials over the last decade—A bibliometric analysis. *Adv. Drug Deliv. Rev.* **2022**, *188*, 114420. [[CrossRef](#)] [[PubMed](#)]
27. Gan, X.; Zhao, H.; Quan, X. Two-dimensional MoS<sub>2</sub>: A promising building block for biosensors. *Biosens. Bioelectron.* **2017**, *89*, 56–71. [[CrossRef](#)] [[PubMed](#)]
28. Samadi, M.; Sarikhani, N.; Zirak, M.; Zhang, H.; Zhang, H.; Moshfegh, A.Z. Group 6 transition metal dichalcogenide nanomaterials: Synthesis, applications and future perspectives. *Nanoscale Horiz.* **2018**, *3*, 90–204. [[CrossRef](#)]
29. Joswig, J.O.; Lorenz, T.; Wendumu, T.B.; Gemming, S.; Seifert, G. Optics, mechanics, and energetics of two-dimensional MoS<sub>2</sub> nanostructures from a theoretical perspective. *Acc. Chem. Res.* **2015**, *48*, 48–55. [[CrossRef](#)]
30. Ataca, C.; Şahin, H.; Ciraci, S. Stable, Single-Layer MX<sub>2</sub> Transition-Metal Oxides and Dichalcogenides in a Honeycomb-Like Structure. *J. Phys. Chem. C* **2012**, *116*, 8983–8999. [[CrossRef](#)]
31. Lee, C.; Yan, H.; Brus, L.E.; Heinz, T.F.; Hone, J.; Ryu, S. Anomalous lattice vibrations of single- and few-layer MoS<sub>2</sub>. *ACS Nano* **2010**, *4*, 2695–2700. [[CrossRef](#)]
32. Huang, Y.; Peng, C.; Chen, R.; Huang, Y.; Ho, C. Transport properties in semiconducting NbS<sub>2</sub> nanoflakes. *Appl. Phys. Lett.* **2014**, *105*, 093106. [[CrossRef](#)]
33. Chen, F.; Xia, J.; Ferry, D.K.; Tao, N. Dielectric screening enhanced performance in graphene FET. *Nano Lett.* **2009**, *9*, 2571–2574. [[CrossRef](#)] [[PubMed](#)]
34. Kalantar-zadeh, K.; Ou, J.Z. Biosensors Based on Two-Dimensional MoS<sub>2</sub>. *ACS Sens.* **2016**, *1*, 5–16. [[CrossRef](#)]
35. Zhang, W.; Zhang, P.; Su, Z.; Wei, G. Synthesis and sensor applications of MoS<sub>2</sub>-based nanocomposites. *Nanoscale* **2015**, *7*, 18364–18378. [[CrossRef](#)]

36. Krishnan, U.; Kaur, M.; Singh, K.; Kumar, M.; Kumar, A. A synoptic review of MoS<sub>2</sub>: Synthesis to applications. *Superlattices Microstruct.* **2019**, *128*, 274–297. [[CrossRef](#)]
37. Andrey, N.; Gotthard Seifert, E. Density-functional study of LixMoS<sub>2</sub> intercalates ( $0 \leq x \leq 1$ ). *Comput. Theor. Chem.* **2012**, *999*, 13–20. [[CrossRef](#)]
38. Mortazavi, M.; Wang, C.; Deng, J.K.; Shenoy, V.B.; Medhekar, N.V. Ab initio characterization of layered MoS<sub>2</sub> as anode for sodium-ion batteries. *J. Power Sources* **2014**, *268*, 279–286. [[CrossRef](#)]
39. Zhao, W.; Pan, J.; Fang, Y.; Che, X.; Wang, D.; Bu, K.; Huang, F. Metastable MoS<sub>2</sub>: Crystal Structure, Electronic Band Structure, Synthetic Approach and Intriguing Physical Properties. *Chemistry* **2018**, *24*, 15942–15954. [[CrossRef](#)]
40. Shi, S.; Sun, Z.; Hu, Y. Synthesis, stabilization and applications of 2-dimensional 1T metallic MoS<sub>2</sub>. *J. Mater. Chem. A* **2018**, *6*, 47. [[CrossRef](#)]
41. Sha, R.; Bhattacharyya, T.K. MoS<sub>2</sub>-based nanosensors in biomedical and environmental monitoring applications. *Electrochim. Acta* **2020**, *349*, 136370. [[CrossRef](#)]
42. Tang, H.; Morrison, S.R. Optimization of the anisotropy of composite MoS<sub>2</sub> films. *Thin Solid Films* **1993**, *227*, 90–94. [[CrossRef](#)]
43. Sundaram, R.S.; Engel, M.; Lombardo, A.; Krupke, R.; Ferrari, A.C.; Avouris, P.; Steiner, M. Electroluminescence in single layer MoS<sub>2</sub>. *Nano Lett.* **2013**, *13*, 1416–1421. [[CrossRef](#)]
44. Kuc, A.; Zibouche, N.; Heine, T. Influence of quantum confinement on the electronic structure of the transition metal sulfide. *Phys. Rev. B* **2011**, *83*, 245213. [[CrossRef](#)]
45. Zhang, X.; Biekert, N.; Choi, S.; Naylor, C.H.; De-Eknamkul, C.; Huang, W.; Zhang, X.; Zheng, X.; Wang, D.; Johnson, A.T.C.; et al. Dynamic Photochemical and Optoelectronic Control of Photonic Fano Resonances via Monolayer MoS<sub>2</sub> Trions. *Nano Lett.* **2018**, *18*, 957–963. [[CrossRef](#)] [[PubMed](#)]
46. Nalwa, H.S. A review of molybdenum disulfide (MoS<sub>2</sub>) based photodetectors: From ultra-broadband, self-powered to flexible devices. *RSC Adv.* **2020**, *10*, 30529–30602. [[CrossRef](#)] [[PubMed](#)]
47. Lee, H.P.; Gaharwar, A.K. Light-Responsive Inorganic Biomaterials for Biomedical Applications. *Adv. Sci.* **2020**, *7*, 2000863. [[CrossRef](#)]
48. Gopalakrishnan, D.; Damien, D.; Shaijumon, M.M. MoS<sub>2</sub> quantum dot-interspersed exfoliated MoS<sub>2</sub> nanosheets. *ACS Nano* **2014**, *8*, 5297–5303. [[CrossRef](#)]
49. Nath, M.; Govindaraj, A.; Rao, C. Simple Synthesis of MoS<sub>2</sub> and WS<sub>2</sub> Nanotubes. *Adv. Mater.* **2001**, *13*, 283–286. [[CrossRef](#)]
50. Lee, H.P.; Lokhande, G.; Singh, K.A.; Jaiswal, M.K.; Rajput, S.; Gaharwar, A.K. Light-Triggered In Situ Gelation of Hydrogels using 2D Molybdenum Disulfide (MoS<sub>2</sub>) Nanoassemblies as Crosslink Epicenter. *Adv. Mater.* **2021**, *33*, e2101238. [[CrossRef](#)]
51. Shounak, R.; Kaivalya, A.D.; Singh, K.A.; Lee, H.P.; Jaiswal, A.; Gaharwar, A.K. Nano-bio interactions of 2D molybdenum disulfide. *Adv. Drug Deliv. Rev.* **2022**, *187*, 114361. [[CrossRef](#)]
52. Najmaei, S.; Yuan, J.; Zhang, J.; Ajayan, P.; Lou, J. Synthesis and defect investigation of two-dimensional molybdenum disulfide atomic layers. *Acc. Chem. Res.* **2015**, *48*, 31–40. [[CrossRef](#)] [[PubMed](#)]
53. Novoselov, K.S.; Fal'ko, V.I.; Colombo, L.; Gellert, P.R.; Schwab, M.G.; Kim, K. A roadmap for graphene. *Nature* **2012**, *490*, 192–200. [[CrossRef](#)]
54. Matte, H.R.; Gomathi, A.; Manna, A.K.; Late, D.J.; Datta, R.; Pati, S.K.; Rao, C.N. MoS<sub>2</sub> and WS<sub>2</sub> analogues of graphene. *Angew. Chem.* **2010**, *49*, 4059–4062. [[CrossRef](#)] [[PubMed](#)]
55. Yao, Y.; Lin, Z.; Lia, Z.; Song, X.; Moona, K.S.; Wong, C. Large-scale production of two-dimensional nanosheets. *J. Mater. Chem.* **2012**, *22*, 13494–13499. [[CrossRef](#)]
56. Forsberg, V.; Zhang, R.; Bäckström, J.; Dahlström, C.; Andres, B.; Norgren, M.; Andersson, M.; Hummelgård, M.; Olin, H. Exfoliated MoS<sub>2</sub> in Water without Additives. *PLoS ONE* **2016**, *11*, e0154522. [[CrossRef](#)] [[PubMed](#)]
57. Varrla, E.; Backes, C.; Paton, K.R.; Harvey, A.; Gholamvand, Z.; McCauley, J.; Coleman, J.N. Large-Scale Production of Size-Controlled MoS<sub>2</sub> Nanosheets by Shear Exfoliation. *Chem. Mater.* **2015**, *27*, 1129–1139. [[CrossRef](#)]
58. Paton, K.R.; Varrla, E.; Backes, C.; Smith, R.J.; Khan, U.; O'Neill, A.; Boland, C.; Lotya, M.; Istrate, O.M.; King, P.; et al. Scalable production of large quantities of defect-free few-layer graphene by shear exfoliation in liquids. *Nat. Mater.* **2014**, *13*, 624–630. [[CrossRef](#)]
59. Zhang, M.; Howe, R.C.T.; Woodward, R.I.; Kelleher, E.J.R.; Torrisi, F.; Hu, G.; Popov, S.V.; Taylor, J.R.; Hasan, T. Solution processed MoS<sub>2</sub>-PVA composite for sub-bandgap mode-locking of a wideband tunable ultrafast Er: fiber laser. *Nano Res.* **2015**, *8*, 1522–1534. [[CrossRef](#)]
60. Liu, N.; Kim, P.; Kim, J.H.; Ye, J.H.; Kim, S.; Lee, C.J. Large-area atomically thin MoS<sub>2</sub> nanosheets prepared using electrochemical exfoliation. *ACS Nano* **2014**, *8*, 6902–6910. [[CrossRef](#)]
61. Coleman, J.N.; Lotya, M.; O'Neill, A.; Bergin, S.D.; King, P.J.; Khan, U.; Young, K.; Gaucher, A.; De, S.; Smith, R.J.; et al. Two-dimensional nanosheets produced by liquid exfoliation of layered materials. *Science* **2011**, *331*, 568–571. [[CrossRef](#)]
62. Eda, G.; Yamaguchi, H.; Voiry, D.; Fujita, T.; Chen, M.; Chhowalla, M. Photoluminescence from chemically exfoliated MoS<sub>2</sub>. *Nano Lett.* **2011**, *11*, 5111–5116. [[CrossRef](#)] [[PubMed](#)]
63. Fan, X.B.; Xu, P.T.; Zhou, D.; Sun, Y.F.; Li, Y.G.C.; Nguyen, M.A.T.; Terrones, M.; Mallouk, T.E. Fast and Efficient Preparation of Exfoliated 2H MoS<sub>2</sub> Nanosheets by Sonication-Assisted Lithium Intercalation and Infrared Laser-Induced 1T to 2H Phase Reversion. *Nano Lett.* **2015**, *15*, 5956–5960. [[CrossRef](#)]

64. Zeng, Z.; Yin, Z.; Huang, X.; Li, H.; He, Q.; Lu, G.; Boey, F.; Zhang, H. Single-Layer Semiconducting Nanosheets: High-Yield Preparation and Device Fabrication. *Angew. Chem. Int. Ed.* **2011**, *50*, 11093–11097. [[CrossRef](#)] [[PubMed](#)]
65. Shi, Y.; Li, H.; Li, L. Recent advances in controlled synthesis of two-dimensional transition metal dichalcogenides via vapour deposition techniques. *Chem. Soc. Rev.* **2015**, *44*, 9. [[CrossRef](#)]
66. Zhan, Y.; Liu, Z.; Najmaei, S.; Ajayan, P.M.; Lou, J. Large-area vapor-phase growth and characterization of MoS<sub>2</sub> atomic layers on a SiO<sub>2</sub> substrate. *Small* **2012**, *8*, 966–971. [[CrossRef](#)]
67. Lin, Y.; Zhang, W.; Huang, J.; Liu, K.; Lee, Y.; Liang, C.; Chu, C.; Li, L. Wafer-scale MoS<sub>2</sub> thin layers prepared by MoO<sub>3</sub> sulfurization. *Nanoscale* **2012**, *4*, 20. [[CrossRef](#)]
68. Endler, I.; Leonhardt, A.; König, U.; van den Berg, H.; Pitschke, W.; Sottke, V. Chemical vapour deposition of MoS<sub>2</sub> coatings using the precursors MoCl<sub>5</sub> and H<sub>2</sub>S. *Surf. Coat. Technol.* **1999**, *120–121*, 482–488. [[CrossRef](#)]
69. Liu, H.; Wong, S.; Chi, D. CVD Growth of MoS<sub>2</sub>-based Two-dimensional Materials. *Chem. Vap. Depos.* **2015**, *21*, 241–259. [[CrossRef](#)]
70. Vattikuti, S.V.P.; Byon, C.; Reddy, C.V.; Venkatesh, B.; Shim, J. Synthesis and structural characterization of MoS<sub>2</sub> nanospheres and nanosheets using solvothermal method. *J. Mater. Sci.* **2015**, *50*, 5024–5038. [[CrossRef](#)]
71. Liao, H.; Wang, Y.; Zhang, S.; Qian, Y. A Solution Low-Temperature Route to MoS<sub>2</sub> Fiber. *Chem. Mater.* **2001**, *6*, 13. [[CrossRef](#)]
72. Jeong, S.; Yoo, D.; Jang, J.; Kim, M.Y.; Cheon, J. Well-Defined Colloidal 2-D Layered Transition-Metal Chalcogenide Nanocrystals via Generalized Synthetic Protocols. *J. Am. Chem. Soc.* **2012**, *134*, 18233–18236. [[CrossRef](#)] [[PubMed](#)]
73. Zhang, Z.; Li, Q.; Du, X.; Liu, M. Application of electrochemical biosensors in tumor cell detection. *Thorac. Cancer* **2020**, *11*, 840–850. [[CrossRef](#)] [[PubMed](#)]
74. Chai, H.; Tang, Y.; Guo, Z.; Miao, P. Ratiometric Electrochemical Switch for Circulating Tumor DNA through Recycling Activation of Blocked DNAzymes. *Anal. Chem.* **2022**, *94*, 2779–2784. [[CrossRef](#)]
75. Manzeli, S.; Dumcenco, D.; Migliato Marega, G.; Kis, A. Self-sensing, tunable monolayer MoS<sub>2</sub> nanoelectromechanical resonators. *Nat. Commun.* **2019**, *10*, 4831. [[CrossRef](#)] [[PubMed](#)]
76. Siao, M.; Shen, W.; Chen, R.; Chang, Z.; Shih, M.; Chiu, Y.; Cheng, C. Two-dimensional electronic transport and surface electron accumulation in MoS<sub>2</sub>. *Nat. Commun.* **2018**, *9*, 1442. [[CrossRef](#)]
77. Tsai, Y.C.; Li, Y. Impact of Doping Concentration on Electronic Properties of Transition Metal-Doped Monolayer Molybdenum Disulfide. *IEEE Trans. Electron. Devices* **2018**, *65*, 733–738. [[CrossRef](#)]
78. Sethulekshmi, A.S.; Saritha, A.; Joseph, K.; Aprem, A.S.; Sisupal, S.B. MoS<sub>2</sub> based nanomaterials: Advanced antibacterial agents for future. *J. Control. Release* **2022**, *348*, 158–185. [[CrossRef](#)]
79. Zhang, S.; Wang, J.; Torad, N.L.; Xia, W.; Aslam, M.A.; Kaneti, Y.V.; Hou, Z.; Ding, Z.; Da, B.; Fatehmulla, A.; et al. Rational Design of Nanoporous MoS<sub>2</sub>/VS<sub>2</sub> Heteroarchitecture for Ultrahigh Performance Ammonia Sensors. *Small* **2020**, *16*, e1901718. [[CrossRef](#)]
80. Ying, Z.; Feng, L.; Ji, D.; Zhang, Y.; Chen, W.; Dai, Y.; Janyasupab, M.; Li, X.; Wen, W.; Liu, C. Phase-Regulated Sensing Mechanism of MoS<sub>2</sub> Based Nanohybrids toward Point-of-Care Prostate Cancer Diagnosis. *Small* **2020**, *16*, e2000307. [[CrossRef](#)]
81. Li, F.; Zhang, L.; Li, J.; Lin, X.; Li, X.; Fang, Y.; Huang, J.; Li, W.; Tian, M.; Jin, J.; et al. Synthesis of Cu–MoS<sub>2</sub>/rGO hybrid as non-noble metal electrocatalysts for the hydrogen evolution reaction. *J. Power Sources* **2015**, *292*, 15–22. [[CrossRef](#)]
82. Su, X.; Han, Y.; Liu, Z.; Fan, L.; Guo, Y. One-pot synthesized AuNPs/MoS<sub>2</sub>/rGO nanocomposite as sensitive electrochemical aptasensing platform for nucleolin detection. *J. Electroanal. Chem.* **2020**, *859*, 113868. [[CrossRef](#)]
83. Jing, P.; Yi, H.; Xue, S.; Chai, Y.; Yuan, R.; Xu, W. A sensitive electrochemical aptasensor based on palladium nanoparticles decorated graphene-molybdenum disulfide flower-like nanocomposites and enzymatic signal amplification. *Chim. Acta* **2015**, *853*, 234–241. [[CrossRef](#)] [[PubMed](#)]
84. Song, Y.; Cao, K.; Li, W.; Ma, C.; Qiao, X.; Li, H.; Hong, C. Optimal film thickness of rGO/MoS<sub>2</sub>@polyaniline nanosheets of 3D arrays for carcinoembryonic antigen high sensitivity detection. *Microchem. J.* **2020**, *155*, 104694. [[CrossRef](#)]
85. Gui, J.; Han, L.; Du, C.; Yu, X.; Hu, K.; Li, L. An efficient label-free immunosensor based on ce-MoS<sub>2</sub>/AgNR composites and screen-printed electrodes for PSA detection. *J. Solid State Electrochem.* **2021**, *25*, 973–982. [[CrossRef](#)]
86. Ma, N.; Zhang, T.; Fan, D.; Kuang, X.; Ali, A.; Wu, D.; Wei, Q. Triple amplified ultrasensitive electrochemical immunosensor for alpha fetoprotein detection based on MoS<sub>2</sub>@Cu<sub>2</sub>O-Au nanoparticles. *Sens. Actuators B Chem.* **2019**, *297*, 126821. [[CrossRef](#)]
87. Ma, E.; Wang, P.; Yang, Q.; Yu, H.; Pei, F.; Li, Y.; Liu, Q.; Dong, Y. Electrochemical immunosensor based on MoS<sub>2</sub> NFs/Au@AgPt YNCs as signal amplification label for sensitive detection of CEA. *Biosens. Bioelectron.* **2019**, *142*, 111580. [[CrossRef](#)]
88. Jia, Q.; Huang, S.; Hu, M.; Song, Y.; Wang, M.; Zhang, Z.; He, L. Polyoxometalate-derived MoS<sub>2</sub> nanosheets embedded around iron-hydroxide nanorods as the platform for sensitively determining miRNA-21. *Sens. Actuators B Chem.* **2020**, *323*, 128647. [[CrossRef](#)]
89. Sri, S.; Chauhan, D.; Lakshmi, G.B.V.S.; Thakar, A.; Solanki, P.R. MoS<sub>2</sub> nanoflower based electrochemical biosensor for TNF alpha detection in cancer patients. *Electrochim. Acta* **2022**, *405*, 139736. [[CrossRef](#)]
90. Hu, T.; Zhang, M.; Wang, Z.; Chen, K.; Li, X.; Ni, Z. Layer-by-layer self-assembly of MoS<sub>2</sub>/PDDA hybrid film in microfluidic chips for ultrasensitive electrochemical immunosensing of alpha-fetoprotein. *Microchem. J.* **2020**, *158*, 105209. [[CrossRef](#)]
91. Hu, D.; Cui, H.; Wang, X.; Luo, F.; Qiu, B.; Cai, W.; Huang, H.; Wang, J.; Lin, Z. Highly Sensitive and Selective Photoelectrochemical Aptasensors for Cancer Biomarkers Based on MoS<sub>2</sub>/Au/GaN Photoelectrodes. *Anal. Chem.* **2021**, *93*, 7341–7347. [[CrossRef](#)]

92. Wei, Q.; Wang, C.; Li, P.; Wu, T.; Yang, N.; Wang, X.; Wang, Y.; Li, C. MOF Photochemistry: ZnS/C/MoS<sub>2</sub> Nanocomposite Derived from Metal–Organic Framework for High-Performance Photo-Electrochemical Immunosensing of Carcinoembryonic Antigen. *Small* **2019**, *15*, 1970257. [[CrossRef](#)]
93. Su, S.; Han, X.; Lu, Z.; Liu, W.; Zhu, D.; Chao, J.; Fan, C.; Wang, L.H.; Song, S.; Weng, L.; et al. Facile Synthesis of a MoS<sub>2</sub>-Prussian Blue Nanocube Nanohybrid-Based Electrochemical Sensing Platform for Hydrogen Peroxide and Carcinoembryonic Antigen Detection. *ACS Appl. Mater. Interfaces* **2017**, *9*, 12773–12781. [[CrossRef](#)] [[PubMed](#)]
94. Wang, Y.; Zhao, G.; Zhang, Y.; Pang, X.; Cao, W.; Du, B.; Wei, Q. Sandwich-type electrochemical immunosensor for CEA detection based on Ag/MoS<sub>2</sub>@Fe<sub>3</sub>O<sub>4</sub> and an analogous ELISA method with total internal reflection microscopy. *Sens. Actuators B Chem.* **2018**, *266*, 561–569. [[CrossRef](#)]
95. Liu, L.; Wei, Y.; Jiao, S.; Zhu, S.; Liu, X. A novel label-free strategy for the ultrasensitive miRNA-182 detection based on MoS<sub>2</sub>/Ti<sub>3</sub>C<sub>2</sub> nanohybrids. *Biosens. Bioelectron.* **2019**, *137*, 45–51. [[CrossRef](#)] [[PubMed](#)]
96. Su, S.; Sun, Q.; Wan, L.; Gu, X.; Zhu, D.; Zhou, Y.; Chao, J.; Wang, L. Ultrasensitive analysis of carcinoembryonic antigen based on MoS<sub>2</sub>-based electrochemical immunosensor with triple signal amplification. *Biosens. Bioelectron.* **2019**, *140*, 111353. [[CrossRef](#)] [[PubMed](#)]
97. Lin, Y.; Xiong, C.; Shi, J.; Zhang, J.; Wang, X. Electrochemical immunosensor based on Pd@Pt/MoS<sub>2</sub>-Gr for the sensitive detection of CEA. *J. Solid. State Electrochem.* **2021**, *25*, 2075–2085. [[CrossRef](#)]
98. Li, S.; Hu, C.; Chen, C.; Zhang, J.; Bai, Y.; Tan, C.; Ni, G.; He, F.; Li, W.; Ming, D. Molybdenum Disulfide Supported on Metal–Organic Frameworks as an Ultrasensitive Layer for the Electrochemical Detection of the Ovarian Cancer Biomarker CA125. *ACS Appl. Bio Mater.* **2021**, *4*, 5494–5502. [[CrossRef](#)]
99. Mehmandoust, M.; Karimi, F.; Erk, N. A zinc oxide nanorods/molybdenum disulfide nanosheets hybrid as a sensitive and reusable electrochemical sensor for determination of anti-retroviral agent indinavir. *Chemosphere* **2022**, *300*, 134430. [[CrossRef](#)]
100. Li, W.; Qiao, X.; Hong, C.; Ma, C.; Song, Y. A sandwich-type electrochemical immunosensor for detecting CEA based on CeO<sub>2</sub>-MoS<sub>2</sub> absorbed Pb<sup>2+</sup>. *Anal. Biochem.* **2020**, *592*, 113566. [[CrossRef](#)]
101. Wang, Y.; Wang, Y.; Wu, D.; Ma, H.; Zhang, Y.; Fan, D.; Pang, X.; Du, B.; Wei, Q. Label-free electrochemical immunosensor based on flower-like Ag/MoS<sub>2</sub>/rGO nanocomposites for ultrasensitive detection of carcinoembryonic antigen. *Sens. Actuators B Chem.* **2018**, *255*, 125–132. [[CrossRef](#)]
102. Gao, Z.; Li, Y.; Zhang, X.; Feng, J.; Kong, L.; Wang, P.; Chen, Z.; Dong, Y.; Wei, Q. Ultrasensitive electrochemical immunosensor for quantitative detection of HBeAg using Au@Pd/MoS<sub>2</sub>@MWCNTs nanocomposite as enzyme-mimetic labels. *Biosens. Bioelectron.* **2018**, *102*, 189–195. [[CrossRef](#)]
103. Pei, F.; Wang, P.; Ma, E.; Yang, Q.; Yu, H.; Liu, J.; Yin, H.; Li, Y.; Liu, Q.; Dong, Y. A sensitive label-free immunosensor for alpha fetoprotein detection using platinum nanodendrites loaded on functional MoS<sub>2</sub> hybridized polypyrrole nanotubes as signal amplifier. *J. Electroanal. Chem.* **2019**, *835*, 197–204. [[CrossRef](#)]
104. Soni, A.; Pandey, C.M.; Pandey, M.K.; Sumana, G. Highly efficient Polyaniline-MoS<sub>2</sub> hybrid nanostructures based biosensor for cancer biomarker detection. *Anal. Chim. Acta* **2019**, *1055*, 26–35. [[CrossRef](#)] [[PubMed](#)]
105. Wang, C.; Wu, T.; Wang, X.; Wei, Q.; Wang, Y.; Li, C.; Sun, D. Ultrathin-layered carbon intercalated MoS<sub>2</sub> hollow nanospheres integrated with gold nanoparticles for photoelectrochemical immunosensing of squamous cell carcinoma antigen. *Sens. Actuators B Chem.* **2019**, *297*, 126716. [[CrossRef](#)]
106. Luo, J.R.; Zeng, Q.; Liu, S.P.; Wei, Q.Y.; Wang, Z.X.; Yang, M.H.; Zou, Y.P.; Lu, L.M. Highly sensitive photoelectrochemical sensing platform based on PM6:Y6 p-n heterojunction for detection of MCF-7 cells. *Sens. Actuators B Chem.* **2022**, *363*, 131814. [[CrossRef](#)]
107. Singh, A.K.; Mittal, S.; Das, M.; Saharia, A.; Tiwari, M. Optical biosensors: A decade in review. *Alex. Eng. J.* **2023**, *67*, 673–691. [[CrossRef](#)]
108. Lv, Q.; Chen, L.; Liu, H.; Zou, L. Peony-like 3D-MoS<sub>2</sub>/graphene nanostructures with enhanced mimic peroxidase performance for colorimetric determination of dopamine. *Talanta* **2022**, *247*, 123553. [[CrossRef](#)]
109. Guo, X.; Wang, Y.; Wu, F.; Ni, Y.; Kokot, S. A colorimetric method of analysis for trace amounts of hydrogen peroxide with the use of the nano-properties of molybdenum disulfide. *Analyst* **2015**, *140*, 1119–1126. [[CrossRef](#)]
110. Zhao, L.; Wang, J.; Su, D.; Zhang, Y.; Lu, H.; Yan, X.; Bai, J.; Gao, Y.; Lu, G. The DNA controllable peroxidase mimetic activity of MoS<sub>2</sub> nanosheets for constructing a robust colorimetric biosensor. *Nanoscale* **2020**, *12*, 19420–19428. [[CrossRef](#)]
111. Su, S.; Li, J.; Yao, Y.; Sun, Q.; Zhao, Q.; Wang, F.; Li, Q.; Liu, X.; Wang, L. Colorimetric Analysis of Carcinoembryonic Antigen Using Highly Catalytic Gold Nanoparticles. *ACS Appl. Bio Mater.* **2019**, *2*, 292–298. [[CrossRef](#)]
112. Wang, X.; Cheng, S.; Wang, X.; Wei, L.; Kong, Q.; Ye, M.; Luo, X.; Xu, J.; Zhang, C.; Xian, Y. pH-Sensitive Dye-Based Nanobio-platform for Colorimetric Detection of Heterogeneous Circulating Tumor Cells. *ACS Sens.* **2021**, *6*, 1925–1932. [[CrossRef](#)] [[PubMed](#)]
113. Ma, C.; Cao, Y.; Gou, X.; Zhu, J. Recent Progress in Electrochemiluminescence Sensing and Imaging. *Anal. Chem.* **2020**, *92*, 431–454. [[CrossRef](#)] [[PubMed](#)]
114. Zhang, S.; Liu, Y. Recent Progress of Novel Electrochemiluminescence Nanoprobes and Their Analytical Applications. *Front. Chem.* **2021**, *8*, 626243. [[CrossRef](#)] [[PubMed](#)]
115. Lv, X.; Li, Y.; Cui, B.; Fang, Y.; Wang, L. Electrochemiluminescent sensor based on an aggregation-induced emission probe for bioanalytical detection. *Analyst* **2022**, *147*, 2338–2354. [[CrossRef](#)] [[PubMed](#)]

116. Du, L.; Zhang, H.; Wang, Z.; Zhuang, T.; Wang, Z. Boosting the electrochemiluminescence of luminol by high-intensity focused ultrasound pretreatment combined with 1T/2H MoS<sub>2</sub> catalysis to construct a sensitive sensing platform. *Ultrason. Sonochem.* **2023**, *92*, 106264. [[CrossRef](#)] [[PubMed](#)]
117. Ma, C.; Zhang, Z.; Tan, T.; Zhu, J. Recent Progress in Plasmonic based Electrochemiluminescence Biosensors: A Review. *Biosensors* **2023**, *13*, 200. [[CrossRef](#)]
118. Zhang, Z.; Yu, H.; Zhang, Y.; Wang, Z.; Gao, H.; Rong, S.; Meng, L.; Dai, J.; Pan, H.; Chang, D. A sandwich-configuration electrochemiluminescence immunoassay based on Cu<sub>2</sub>O@OMC-Ru nanocrystals and OMC-MoS<sub>2</sub> nanocomposites for determination of alpha-fetoprotein. *Mikrochim. Acta* **2021**, *188*, 213. [[CrossRef](#)]
119. Srinidhi, G.; Sudalaimani, S.; Giribabu, K.; Basha, S.J.S.; Suresh, C. Amperometric determination of hydrazine using a CuS-ordered mesoporous carbon electrode. *Mikrochim. Acta* **2020**, *187*, 359. [[CrossRef](#)]
120. Liu, Y.; Nie, Y.; Wang, M.; Zhang, Q.; Ma, Q. Distance-dependent plasmon-enhanced electrochemiluminescence biosensor based on MoS<sub>2</sub> nanosheets. *Biosens. Bioelectron.* **2020**, *148*, 111823. [[CrossRef](#)]
121. Muhammad, M.; Khan, S.; Shehzadi, S.A.; Gul, Z.; Al-Saidi, H.M.; Kamran, A.W.; Alhumaydhi, F.A. Recent advances in colorimetric and fluorescent chemosensors based on thiourea derivatives for metallic cations: A review. *Dye. Pigment.* **2022**, *205*, 110477. [[CrossRef](#)]
122. Yao, W.; Ling, J.; Zhang, W.; Ding, Y. Highly sensitive fluorescent aptasensor based on MoS<sub>2</sub> nanosheets for one-step determination of methamphetamine. *Anal. Sci.* **2022**, *38*, 99–104. [[CrossRef](#)] [[PubMed](#)]
123. Liang, J.; Yan, R.; Chen, C.; Yao, X.; Guo, F.; Wu, R.; Zhou, Z.; Chen, J.; Li, G. A novel fluorescent strategy for Golgi protein 73 determination based on aptamer/nitrogen-doped graphene quantum dots/molybdenum disulfide @ reduced graphene oxide nanosheets. *Spectrochim. Acta A Mol. Biomol. Spectrosc.* **2023**, *294*, 122538. [[CrossRef](#)] [[PubMed](#)]
124. Wang, J.; Liu, Y.; Ding, Z.; Zhang, L.; Han, C.; Yan, C.; Amador, E.; Yuan, L.; Wu, Y.; Song, C.; et al. The exploration of quantum dot-molecular beacon based MoS<sub>2</sub> fluorescence probing for myeloma-related Mirnas detection. *Bioact. Mater.* **2022**, *17*, 360–368. [[CrossRef](#)] [[PubMed](#)]
125. Chhowalla, M.; Shin, H.S.; Eda, G.; Li, L.J.; Loh, K.P.; Zhang, H. The chemistry of two-dimensional layered transition metal dichalcogenide nanosheets. *Nat. Chem.* **2013**, *5*, 263–275. [[CrossRef](#)] [[PubMed](#)]
126. Ge, J.; Hu, Y.; Deng, R.; Li, Z.; Zhang, K.; Shi, M.; Yang, D.; Cai, R.; Tan, W. Highly Sensitive MicroRNA Detection by Coupling Nicking-Enhanced Rolling Circle Amplification with MoS<sub>2</sub> Quantum Dots. *Anal. Chem.* **2020**, *92*, 13588–13594. [[CrossRef](#)]
127. Strobbia, P.; Cupil-Garcia, V.; Crawford, B.M.; Fales, A.M.; Pfefer, T.J.; Liu, Y.; Maiwald, M.; Sumpf, B.; Vo-Dinh, T. Accurate in vivo tumor detection using plasmonic-enhanced shifted-excitation Raman difference spectroscopy (SERDS). *Theranostics* **2021**, *11*, 4090–4102. [[CrossRef](#)] [[PubMed](#)]
128. Er, E.; Sánchez-Iglesias, A.; Silvestri, A.; Arnaiz, B.; Liz-Marzán, L.M.; Prato, M.; Criado, A. Metal Nanoparticles/MoS<sub>2</sub> Surface-Enhanced Raman Scattering-Based Sandwich Immunoassay for  $\alpha$ -Fetoprotein Detection. *ACS Appl. Mater. Interfaces* **2021**, *13*, 8823–8831. [[CrossRef](#)]
129. Pan, H.; Dong, Y.; Gong, L.; Zhai, J.; Song, C.; Ge, Z.; Su, Y.; Zhu, D.; Chao, J.; Su, S.; et al. Sensing gastric cancer exosomes with MoS<sub>2</sub>-based SERS aptasensor. *Biosens. Bioelectron.* **2022**, *215*, 114553. [[CrossRef](#)]
130. Medetalibeyoglu, H.; Kotan, G.; Atar, N.; Yola, M.L. A novel sandwich-type SERS immunosensor for selective and sensitive carcinoembryonic antigen (CEA) detection. *Anal. Chim. Acta* **2020**, *1139*, 100–110. [[CrossRef](#)]
131. Samy, O.; Zeng, S.; Birowosuto, M.D.; El Moutaouakil, A. A Review on MoS<sub>2</sub> Properties, Synthesis, Sensing Applications and Challenges. *Crystals* **2021**, *11*, 355. [[CrossRef](#)]
132. Chiu, N.F.; Yang, H.T. High-Sensitivity Detection of the Lung Cancer Biomarker CYFRA21-1 in Serum Samples Using a Carboxyl-MoS<sub>2</sub> Functional Film for SPR-Based Immunosensors. *Front. Bioeng. Biotechnol.* **2020**, *8*, 234. [[CrossRef](#)] [[PubMed](#)]
133. Xin, W.; Jiang, L.; Zong, L.; Zeng, H.; Shu, G.; Marks, R.; Zhang, X.; Shan, D. MoS<sub>2</sub> quantum dots-combined zirconium-metalloporphyrin frameworks: Synergistic effect on electron transfer and application for bioassay. *Sens. Actuators B Chem.* **2018**, *273*, 566–573. [[CrossRef](#)]
134. Hou, F.; Hu, X.; Ma, S.; Cao, J.; Liu, Y. Construction of electrochemiluminescence sensing platform with in situ generated coreactant strategy for sensitive detection of prostate specific antigen. *J. Electroanal. Chem.* **2020**, *858*, 113817. [[CrossRef](#)]
135. Nie, Y.; Zhang, X.; Zhang, Q.; Liang, Z.; Ma, Q.; Su, X. A novel high efficient electrochemiluminescence sensor based on reductive Cu(I) particles catalyzed Zn-doped MoS<sub>2</sub> QDs for HPV 16 DNA determination. *Biosens. Bioelectron.* **2020**, *160*, 112217. [[CrossRef](#)] [[PubMed](#)]
136. Hou, S.; Wang, P.; Nie, Y.; Guo, Y.; Ma, Q. A novel work function tuning strategy-based ECL sensor with sulfur dots and Au NP@MoS<sub>2</sub> nanosheet heterostructure for triple-negative breast cancer diagnosis. *Chem. Eng. J.* **2022**, *446*, 136906. [[CrossRef](#)]
137. Liu, W.; Su, M.; Chen, A.; Peng, K.; Chai, Y.; Yuan, R. Highly Efficient Electrochemiluminescence Based on Luminol/MoS<sub>2</sub> Quantum Dots@Zeolitic Imidazolate Framework-8 as an Emitter for Ultrasensitive Detection of MicroRNA. *Anal. Chem.* **2022**, *94*, 9106–9113. [[CrossRef](#)]
138. Zhao, L.; Kong, D.; Wu, Z.; Liu, G.; Gao, Y.; Yan, X.; Liu, F.; Liu, X.; Wang, C.; Cui, J.; et al. Interface interaction of MoS<sub>2</sub> nanosheets with DNA based aptameric biosensor for carbohydrate antigen 15–3 detection. *Microchem. J.* **2020**, *155*, 104675. [[CrossRef](#)]
139. Peng, X.; Wang, Y.; Wen, W.; Chen, M.; Zhang, X.; Wang, S. Simple MoS<sub>2</sub>-Nanofiber Paper-Based Fluorescence Immunosensor for Point-of-Care Detection of Programmed Cell Death Protein 1. *Anal. Chem.* **2021**, *93*, 8791–8798. [[CrossRef](#)]

140. Jiang, J.; Liu, H.; Li, X.; Chen, Y.; Gu, C.; Wei, G.; Zhou, J.; Jiang, T. Nonmetallic SERS-based immunosensor by integrating MoS<sub>2</sub> nanoflower and nanosheet towards the direct serum detection of carbohydrate antigen 19-9. *Biosens. Bioelectron.* **2021**, *193*, 113481. [CrossRef]
141. Van der Zande, A.M.; Huang, P.S.Y.; Chenet, D.A.; Berkelbach, T.C.; You, Y.M.; Lee, G.H.; Heinz, T.F.; Reichman, D.R.; Muller, D.A.; Hone, J.C. Grains and grain boundaries in highly crystalline monolayer molybdenum disulfide. *Nat. Mater.* **2013**, *12*, 554–561. [CrossRef]
142. Shi, J.; Qin, W.; Lin, Y.; Li, M.; Wu, Y.; Luo, H.; Yan, J.; Huang, K.; Tan, X. Enhancing biosensing with fourfold amplification and self-powering capabilities: MoS<sub>2</sub>@C hollow nanorods-mediated DNA hexahedral framework architecture for amol-level liver cancer tumor marker detection. *Anal. Chim. Acta* **2023**, *1271*, 341413. [CrossRef] [PubMed]
143. Wang, R.; Liu, H.; Xu, T.; Zhang, Y.; Gu, C.; Jiang, T. SERS-based recyclable immunoassay mediated by 1T-2H mixed-phase magnetic molybdenum disulfide probe and 2D graphitic carbon nitride substrate. *Biosens. Bioelectron.* **2023**, *227*, 115160. [CrossRef] [PubMed]
144. Yang, Y.; Zeng, B.; Li, Y.; Liang, H.; Yang, Y.; Yuan, Q. Construction of MoS<sub>2</sub> field effect transistor sensor array for the detection of bladder cancer biomarkers. *Sci. China Chem.* **2020**, *63*, 997–1003. [CrossRef]
145. Zhang, Y.; Feng, D.; Xu, Y.; Yin, Z.; Dou, W.; Habiba, U.M.E.; Pan, C.; Zhang, Z.; Mou, H.; Deng, H.; et al. DNA-based functionalization of two-dimensional MoS<sub>2</sub> FET biosensor for ultrasensitive detection of PSA. *Appl. Surf. Sci.* **2021**, *548*, 149169. [CrossRef]
146. Negahdary, M.; Angnes, L. Recent advances in electrochemical nanomaterial-based aptasensors for the detection of cancer biomarkers. *Talanta* **2023**, *259*, 124548. [CrossRef] [PubMed]
147. Shi, J.; Song, Y.; Lin, Y.; Wu, Y.; Luo, H.; Yan, J.; Huang, K.; Tan, X. Sensitive detection of cancer biomarker with enzyme-free mediated cascade signal amplification empowered undisturbed dual-mode assay. *Sens. Actuators B Chem.* **2023**, *394*, 134430. [CrossRef]
148. Hou, Y.; Xu, J.; Xie, W.; Huang, K.; Tan, X.; Zhao, B.; Zhang, S.; Gao, M. 3D DNA walker recognition-driven homogeneous dual-mode sensing strategy based on enzyme biofuel cell for ultrasensitive detection of HER2. *Sens. Actuators B Chem.* **2023**, *376* (Pt B), 132998. [CrossRef]
149. Lee, M.; Park, S.J.; Kim, G.; Park, C.; Lee, M.H.; Ahn, J.H.; Lee, T. A pretreatment-free electrical capacitance biosensor for exosome detection in undiluted serum. *Biosens. Bioelectron.* **2022**, *199*, 113872. [CrossRef]
150. Kashefi-Kheyraadi, L.; Kim, J.; Chakravarty, S.; Park, S.y.; Gwak, H.; Kim, S.; Mohammadniaei, M.; Lee, M.H.; Hyun, K.A.; Jung, H. Detachable microfluidic device implemented with electrochemical aptasensor (DeMEA) for sequential analysis of cancerous exosomes. *Biosens. Bioelectron.* **2020**, *169*, 112622. [CrossRef]
151. Yagati, A.K.; Go, A.; Vu, N.H.; Lee, M.H. A MoS<sub>2</sub>-Au nanoparticle-modified immunosensor for T3 biomarker detection in clinical serum samples. *Electrochim. Acta* **2020**, *342*, 136065. [CrossRef]
152. Jandas, P.J.; Luo, J.; Prabakaran, K.; Chen, F.; Fu, Y. Highly stable, love-mode surface acoustic wave biosensor using Au nanoparticle-MoS<sub>2</sub>-rGO nano-cluster doped polyimide nanocomposite for the selective detection of carcinoembryonic antigen. *Mater. Chem. Phys.* **2020**, *246*, 122800. [CrossRef]
153. Torul, H.; Yarali, E.; Eksin, E.; Ganguly, A.; Benson, J.; Tamer, U.; Papakonstantinou, P.; Erdem, A. Paper-Based Electrochemical Biosensors for Voltammetric Detection of miRNA Biomarkers Using Reduced Graphene Oxide or MoS<sub>2</sub> Nanosheets Decorated with Gold Nanoparticle Electrodes. *Biosensors* **2021**, *11*, 236. [CrossRef] [PubMed]
154. Zhou, C.; Cui, K.; Liu, Y.; Li, L.; Zhang, L.; Hao, S.; Ge, S.; Yu, J. Bi<sub>2</sub>S<sub>3</sub>@MoS<sub>2</sub> Nanoflowers on Cellulose Fibers Combined with Octahedral CeO<sub>2</sub> for Dual-Mode Microfluidic Paper-Based MiRNA-141 Sensors. *ACS Appl. Mater. Interfaces* **2021**, *13*, 32780–32789. [CrossRef] [PubMed]
155. Ma, J.; Xue, D.; Xu, T.; Wei, G.; Gu, C.; Zhang, Y.; Jiang, T. Nonmetallic SERS-based biosensor for ultrasensitive and reproducible immunoassay of ferritin mediated by magnetic molybdenum disulfide nanoflowers and black phosphorus nanosheets. *Colloids Surf. B Biointerfaces* **2023**, *227*, 113338. [CrossRef]
156. Yan, R.; Lu, N.; Han, S.; Lu, Z.; Xiao, Y.; Zhao, Z.; Zhang, M. Simultaneous detection of dual biomarkers using hierarchical MoS<sub>2</sub> nanostructuring and nano-signal amplification-based electrochemical aptasensor toward accurate diagnosis of prostate cancer. *Biosens. Bioelectron.* **2022**, *197*, 113797. [CrossRef]
157. Shi, J.; Zhang, Y.; Wang, P.; Nie, Y.; Ma, Q. Luminous MoS<sub>2</sub> nanosheet-based electrochemiluminescence biosensor with biomimetic vesicle for miRNA-210 detection. *Talanta* **2022**, *237*, 122969. [CrossRef]
158. Wang, X.; Ji, J.; Yang, P.; Li, X.; Pang, Y.; Lu, P. A love-mode surface acoustic wave aptasensor with dummy fingers based on monolayer MoS<sub>2</sub>/Au NPs nanocomposites for alpha-fetoprotein detection. *Talanta* **2022**, *243*, 123328. [CrossRef]
159. Sun, Z.W.; Tong, Y.; Zhao, L.; Li, J.; Gao, F.C.; Wang, C.X.; Li, H.; Du, L.T.; Jiang, Y.Y. MoS<sub>2</sub>@Ti<sub>3</sub>C<sub>2</sub> nanohybrid-based photoelectrochemical biosensor: A platform for ultrasensitive detection of cancer biomarker exosomal miRNA. *Talanta* **2022**, *238*, 123077. [CrossRef]
160. Rus, L.; Tertis, M.; Pop, A.; Fizeşan, L.; Bogdan, D.; Matei, E.; Oprea, D.; Diculescu, V.; Săndulescu, R.; Cristea, C. The use of a new selective AB3 aptamer for the hematologic tumor cells' detection. *Sens. Actuators B Chem.* **2023**, *394*, 134389. [CrossRef]
161. Majd, S.M.; Mirzapour, F.; Shamsipur, M.; Manouchehri, I.; Babaee, E.; Pashabadi, A.; Moradian, R. Design of a novel aptamer/molecularly imprinted polymer hybrid modified Ag-Au@Insulin nanoclusters/Au-gate-based MoS<sub>2</sub> nanosheet field-effect transistor for attomolar detection of BRCA1 gene. *Talanta* **2023**, *257*, 124394. [CrossRef]

162. Guo, Y.; Nie, Y.; Wang, P.; Li, Z.; Ma, Q. MoS<sub>2</sub> QDs-MXene heterostructure-based ECL sensor for the detection of miRNA-135b in gastric cancer exosomes. *Talanta* **2023**, *259*, 124559. [[CrossRef](#)] [[PubMed](#)]
163. Rahman, M.T.; Kumar, R.; Kumar, M.; Qiao, Q.Q. Two-dimensional transition metal dichalcogenides and their composites for lab-based sensing applications: Recent progress and future outlook. *Sens. Actuators A Phys.* **2021**, *318*, 112517. [[CrossRef](#)]
164. Nakada, G.; Igarashi, Y.; Imai, H.; Oaki, Y. Materials-Informatics-Assisted High-Yield Synthesis of 2D Nanomaterials through Exfoliation. *Adv. Theory Simul.* **2019**, *2*, 1800180. [[CrossRef](#)]
165. Hu, T.; Zhang, R.; Li, J.; Cao, J.; Qiu, F. Photodetectors based on two-dimensional MoS<sub>2</sub> and its assembled heterostructures. *Chip* **2022**, *1*, 100017. [[CrossRef](#)]
166. Kaur, J.; Singh, M.; Dell'Aversana, C.; Benedetti, R.; Giardina, P.; Rossi, M.; Valadan, M.; Vergara, A.; Cutarelli, A.; Montone, A.M.I.; et al. Biological interactions of biocompatible and water-dispersed MoS<sub>2</sub> nanosheets with bacteria and human cells. *Sci. Rep.* **2018**, *68*, 16386. [[CrossRef](#)]
167. Mohan, M.; Shetti, N.P.; Aminabhavi, T.M. Recent developments in MoS<sub>2</sub>-based flexible supercapacitors. *Materials Today Chem.* **2023**, *27*, 101333. [[CrossRef](#)]

**Disclaimer/Publisher's Note:** The statements, opinions and data contained in all publications are solely those of the individual author(s) and contributor(s) and not of MDPI and/or the editor(s). MDPI and/or the editor(s) disclaim responsibility for any injury to people or property resulting from any ideas, methods, instructions or products referred to in the content.